Inorg. Chem. **2005**, *44*, 1248–1262

Structural Properties and Dissociative Fluxional Motion of 2,9-Dimethyl-1,10-Phenanthroline in Platinum(II) Complexes

Raffaello Romeo,*,† Salvatore Carnabuci,† Maria Rosaria Plutino,‡ Andrea Romeo,† Silvia Rizzato,§ and Alberto Albinati§

Dipartimento di Chimica Inorganica, Chimica Analitica e Chimica Fisica, Università di Messina, Salita Sperone 31, Vill. S. Agata 98166, Messina, Italy, Istituto Materiali Nanostrutturati, ISMN - CNR, Unità di Messina, Sezione di Palermo, Italy, and Dipartimento di Chimica Strutturale (DCSSI) e Facoltà di Farmacia, via Venezian 21, Università di Milano, Milano, Italy

Received October 8, 2004

A dynamic ^{1}H NMR study has been carried out on the fluxional motion of the symmetric chelating ligand 2,9-dimethyl-1,10-phenanthroline (Me_2-phen) between nonequivalent exchanging sites in a variety of square-planar complexes of the type [Pt(Me)(Me_2-phen)(PR_3)]BArf, **1**–**14**, (BArf = B[3,5-$(CF_3)_2C_6H_3]_4$). In these compounds, the P-donor ligands PR_3 encompass a wide range of steric and electronic characteristics [PR_3 = P(4-$XC_6H_4)_3$, X = H **1**, F, **2**, Cl **3**, CF_3 **4**, MeO **5**, Me **6**; PR_3 = $PMe(C_6H_5)_2$ **7**, $PMe_2(C_6H_5)$ **8**, PMe_3 **9**, PEt_3 **10**, P(*i*-Pr)$_3$ **11**, $PCy(C_6H_5)_2$ **12**, $PCy_2(C_6H_5)$ **13**, PCy_3 **14**]. All complexes have been synthesized and fully characterized through elemental analysis, ^{1}H and ^{31}P{^{1}H} NMR. X-ray crystal structures are reported for the compounds **8**, **11**, **14**, and for [Pt(Me)(phen)(P$(C_6H_5)_3$)]PF_6 (**15**), all but the last showing loss of planarity and a significant rotation of the Me_2-phen moiety around the N1–N2 vector. Steric congestion brought about by the P-donor ligands is responsible for tetrahedral distortion of the coordination plane and significant lengthening of the Pt–N_2 (cis to phosphane) bond distances. Application of standard quantitative analysis of ligand effects (QALE) methodology enabled a quantitative separation of steric and electronic contributions of P-donor ligands to the values of the platinum–phosphorus $^1J_{PtP}$ coupling constants and of the free activation energies $\Delta G^{\ddagger}$ of the fluxional motion of Me_2-phen in **1**–**14**. The steric profiles for both $^1J_{PtP}$ and $\Delta G^{\ddagger}$ show the onset of steric thresholds (at cone angle values of 150° and 148°, respectively), that are associated with an overload of steric congestion already evidenced by the crystal structures of **11** and **14**. The sharp increase of the fluxional rate of Me_2-phen can be assumed as a perceptive kinetic tool for revealing ground-state destabilization produced by the P-donor ligands. The mechanism involves initial breaking of a metal–nitrogen bond, fast interconversion between two 14-electron three-coordinate T-shaped intermediates containing η^1-coordinated Me_2-phen, and final ring closure. By use of the results from QALE regression analysis, a free-energy surface has been constructed that represents the way in which any single P-donor ligand can affect the energy of the transition state in the absence of aryl or π-acidity effects.

Introduction

The bidentate nitrogen ligand 2,9-dimethyl-1,10-phenanthroline (Me_2-phen), when coordinated to monoalkyl cationic platinum(II) complexes of the type [Pt(Me)(Me_2-phen)(L)]$^+$, exhibits a fast fluxional motion between two nonequivalent exchanging sites.[1,2] The origin of the phenomenon is mainly steric in nature. Steric hindrance brought by the methyl substituents of Me_2-phen in proximity to other groups coordinated to the metal favors a pronounced distortion of the ligand that is observed in a number of X-ray studies of similar compounds.[3] This distortion may be measured by the dihedral angle between the plane of the chelating moiety and that of the square-planar coordination plane. For instance, the complex [Pt(Me)(Me_2-phen)(Me_2SO)]$^+$ exhibits a flux-

* Author to whom correspondence should be addressed. E-mail: Raf.Romeo@chem.unime.it. Fax: ++39-090-393756. Phone: ++39-090-6765717.

† Università di Messina.

‡ Istituto Materiali Nanostrutturati.

§ Università di Milano.

(1) Romeo, R.; Fenech, L.; Monsù Scolaro, L.; Albinati, A.; Macchioni, A.; Zuccaccia, C. *Inorg. Chem.* **2001**, *40*, 3293−3302.

(2) Romeo, R.; Fenech, L.; Carnabuci, S.; Plutino, M. R.; Romeo, A. *Inorg. Chem.* **2002**, *41*, 2839−2847.

10.1021/ic0485920 CCC: $30.25
Published on Web 02/10/2005

ional behavior while $[Pt(Me)(phen)(Me_2SO)]^+$, with the phenanthroline plane lying almost coplanar with the coordination plane,[4] features a static structure. In the substrate containing Me_2-phen, the same specific nonbonding repulsions by the 2,9 methyl groups that promote the chelate flipping must be held responsible for the high lability of Me_2-SO. The ligand exchange with uncoordinated Me_2SO takes place at a rate ($k_2 = 38 \times 10^3\ m^{-1}s^{-1}$) that is 5 orders of magnitude higher than that of the complex containing unsubstituted phen ($k_2 = 0.18\ m^{-1}s^{-1}$) or even of complexes with alkyl or aryl substituents at the periphery of phenanthroline (3,4,7,8-Me_4phen, $k_2 = 0.026\ m^{-1}s^{-1}$; 4,7-$Ph_2$phen, $k_2 = 0.10\ m^{-1}s^{-1}$).[5] This represents a rare, if not a unique, case of steric acceleration in associative nucleophilic substitutions at square-planar complexes, accounted for by the propensity of the dinitrogen ligand to form a flat unconstrained five-membered ring in the trigonal plane of the five-coordinate intermediate. Steric relief is also at the origin of the easy direct uptake of strong π-acceptor ligands, such as alkene or alkyne by $[PtX_2(Me_2\text{-phen})]$ (X = halide ions) complexes to form discrete and stable five-coordinate trigonal bipyramidal species.[6−8]

On substituting Me_2SO with a firmly bonded ligand, as in $[Pt(Me)(Me_2\text{-phen})(PPh_3)]^+$ (**1**), ligand exchange is blocked and the only possible dynamic motion remains the flipping of Me_2-phen that was previously investigated by variable-temperature NMR spectroscopy in $CDCl_3$ as a function of the counteranion, the solvent, or of added nucleophiles.[1,2] The high trans effect and trans influence of the methyl and phosphane groups, together with the remarkable steric congestion at the coordination plane, favor either a facile dissociation of a Pt−N bond or the addition of a fifth group. Thus, the mechanism is switchable between intramolecular dissociative and bimolecular associative pathways, depending on the interionic structure of the complex and the action of potential nucleophiles. The first process is prevalent within the ion pairs, detected by $^{19}F\{^1H\}$ HOESY NMR spectra and formed by "noncoordinating" anions (X = PF_6^-, BF_4^-, etc.) with the cationic complex in nonpolar solvents.[1] Among the possible associative mechanisms promoted by polar solvents or by relatively strong nucleophiles such as sulfides or sulfoxides, a consecutive stepwise displacement mechanism is preferred to intramolecular rearrangements (Berry pseudorotation or turnstile) of five-coordinated intermediates.[2] Both dissociative and associative mechanisms involve ring opening and Pt−N bond rupture.

Compounds similar to **1**, where PPh_3 has been substituted by less efficient trans-activating groups L (amine, pyridine, or thiourea), behave as stereochemically rigid N−N chelate complexes.[1] This indicates that electronic factors also come into play and are connected to the capacity of the ligand L of promoting Pt−N bond dissociation. Within this mechanistic framework, we thought it could be worthwhile to extend our previous study to the fluxionality of $[Pt(Me)(Me_2\text{-phen})(L)]^+$ complexes, including P-donor ligands with widely different electronic and steric properties. Moreover, the application of QALE methodology enabled the rate constants and the NMR data to be analyzed according to the electronic and steric characteristics of the ligands.

Results

Synthesis and General Properties. The complex $[Pt(Me)(Me_2\text{-phen})(Me_2SO)]PF_6$, prepared following a published procedure,[5] was used as a useful synthon for the formation of the corresponding salts containing a wide series of P-donor ligands, taking advantage of the easy removal of Me_2SO by phosphanes, according to the substitution reaction

$$[Pt(Me)(Me_2\text{-phen})(Me_2SO)]PF_6 + PR_3 \rightarrow [Pt(Me)(Me_2\text{-phen})(PR_3)]PF_6 + Me_2SO \quad (1)$$

The hexafluorophosphate salts thus obtained were converted into the final $[Pt(Me)(Me_2\text{-phen})(PR_3)]BArf$ (BArf = $B[3,5\text{-}(CF_3)_2C_6H_3]_4$) compounds **1**−**14** by treatment with Na(BArf) and separation of $NaPF_6$. The anion exchange of BArf for PF_6 was dictated by the well-known noncoordinating properties of BArf and the necessity of avoiding any possible interaction of the anion with the metal−cationic complex in solution. Actually, the $^{19}F\{^1H\}$ HOESY spectrum of $[Pt(Me)(Me_2\text{-phen})(PPh_3)]$ BArf **1**, recorded at 260 K in $CDCl_3$, showed the absence of interionic contacts between the fluorine atoms of CF_3 groups of BArf and hydrogen atoms of the cation, indicating that the compound in chloroform is not appreciably present as an intimate ion pair.[1]

X-ray Structural Studies. ORTEP views of the cations **8**, **11**, **14**, and **15** are shown in Figure 1, Figure 2, Figure 3, and Figure 4, respectively. A list of relevant bond distances and angles is given in Table 1. Compound **15**, in which an unsubstituted phenanthroline moiety (*phen*) is bound to the Pt atom, may be used, by comparison to the other compounds, to show the effect of the methyl substitution in position 2,9 on the geometry of the complexes. It is worth

(3) (a) Klein, A.; McInnes, E. J. L.; Kaim, W. *J. Chem. Soc., Dalton Trans.* **2002**, 2371−2378. (b) Clark, R. J. H.; Fanizzi, F. P.; Natile, G.; Pacifico, C.; van Rooyen, C. G.; Tocher, D. A. *Inorg. Chim. Acta* **1995**, *235*, 205−213. (c) Fanizzi, F. P.; Intini, F. P.; Maresca, L.; Natile, G.; Lanfranchi, M.; Tiripicchio, A. *J. Chem. Soc., Dalton Trans.* **1991**, 1007−1015. (d) Fanizzi, F. P.; Natile, G.; Lanfranchi, M.; Tiripicchio, A.; Laschi, F.; Zanello, P. *Inorg. Chem.* **1996**, *35*, 3173−3182. (e) De Felice, V.; Albano, V. G.; Castellari, C.; Cucciolito, M. E.; De Renzi, A. *J. Organomet. Chem.* **1991**, *403*, 269−277. (f) Milani, B.; Alessio, E.; Mestroni, G.; Sommazzi, A.; Garbassi, F.; Zangrando, E.; Bresciani-Pahor, N.; Randaccio, L. *J. Chem. Soc., Dalton Trans.* **1994**, 1903−1911. (g) Cucciolito, M. E.; De Renzi, A.; Giordano, F.; Ruffo, F. *Organometallics* **1995**, *14*, 5410−5414.

(4) Bruno, G.; Nicolò, F.; Scopelliti, R.; Arena, G. *Acta Crystallogr., Sect. C* **1996**, *52*, 827−829.

(5) Romeo, R.; Monsù Scolaro, L.; Nastasi, N.; Arena, G. *Inorg. Chem.* **1996**, *35*, 5087−5096.

(6) (a) Albano, V. G.; Natile, G.; Panunzi, A. *Coord. Chem. Rev.* **1994**, *133*, 67−114. (b) Maresca, L.; Natile, G. *Comments Inorg. Chem.* **1993**, *14*, 349−366.

(7) (a) Albano, V. G.; Ferrara, M. L.; Monari, M.; Panunzi, A.; Ruffo, F. *Inorg. Chim. Acta* **1999**, *285*, 70−75. (b) De Felice, V.; Ferrara, M. L.; Giordano, F.; Ruffo, F. *Gazz. Chim. Ital.* **1994**, *124*, 117−119. (c) Giordano, F.; Ruffo, F.; Saporito, A.; Panunzi, A. *Inorg. Chim. Acta* **1997**, *264*, 231−237. (d) Fanizzi, F. P.; Natile, G.; Lanfranchi, M.; Tiripicchio, A.; Pacchioni, G. *Inorg. Chim. Acta* **1998**, *275*, 500−509. (e) Albano, V. G.; Castellari, C.; Monari, M.; De Felice, V.; Panunzi, A.; Ruffo, F. *Organometallics* **1996**, *15*, 4012−4019. (f) Albano, V. G.; Castellari, C.; Monari, M.; De Felice, V.; Panunzi, A.; Ruffo, F. *Organometallics* **1992**, *11*, 3665−3669.

(8) Fanizzi, F. P.; Margiotta, N.; Lanfranchi, M.; Tiripicchio, A.; Pacchioni, G.; Natile, G. *Eur. J. Inorg. Chem.* **2004**, *8*, 1705−1713.

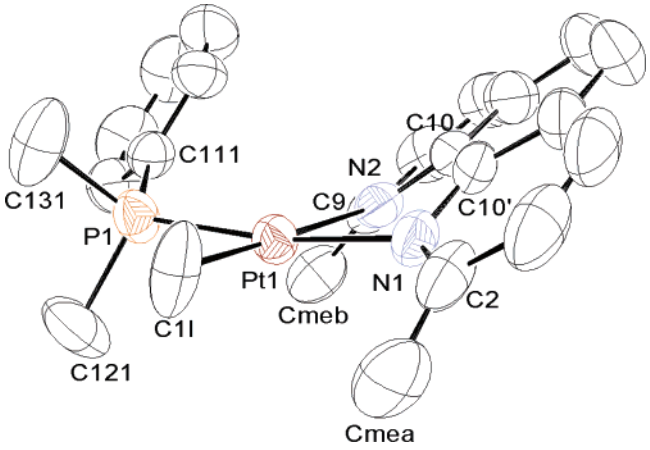

Figure 1. ORTEP view of the cation **8** showing 50% probability ellipsoids.

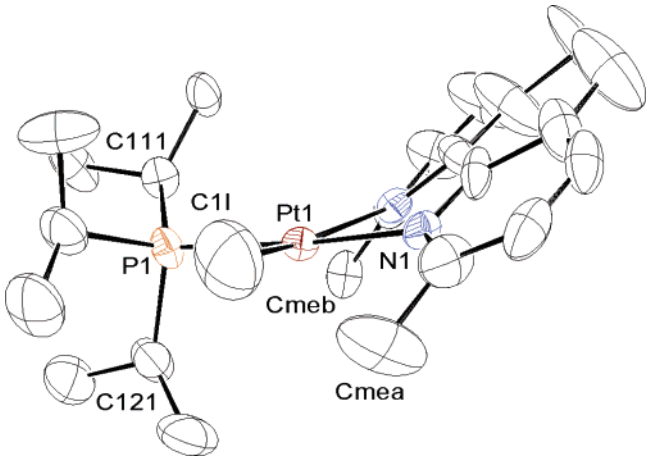

Figure 2. ORTEP view of the cation **11** showing 50% probability ellipsoids.

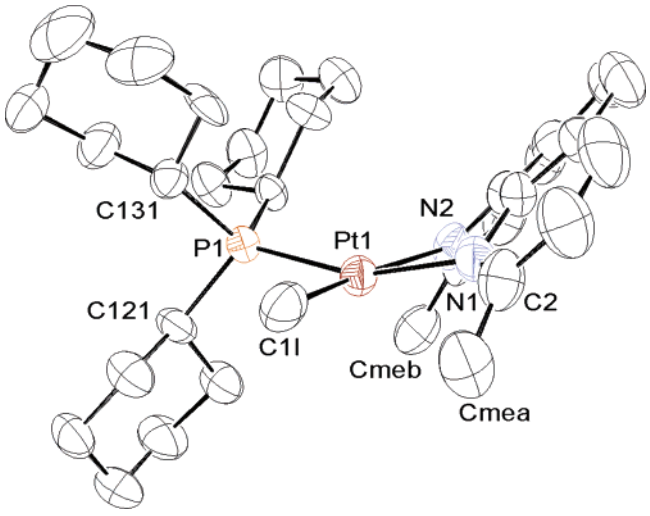

Figure 3. ORTEP view of the cation **14** showing 50% probability ellipsoids.

noticing that, in compound **15**, there are three independent molecules in the asymmetric unit. There are no significant differences in the coordination geometries, with the exception of the relative orientation of the phenyl rings of the phosphane (cf. the Pt−P1−C111−C112 torsion angles in Table 1) possibly because of the packing constraints. The relative arrangement of the three independent molecules (Figure 4) shows planar *phen* moieties arranged to form a "supra-unit" held together by attractive $\pi-\pi$ stacking interactions (inter-ring shortest distances in the range 3.5−3.7 Å), with no Pt···Pt interactions ($d_{Pt-Pt} \geq 8.5$ Å). There are no relevant distortions from the square-planar coordination as shown by the deviation from the coordination plane (defined by the atoms Pt, P, N1, N2, C1L) of ca. ±0.04 Å.

An important feature of the Me_2-phen cations **1**, **8**, **11**, and **14** is that the differences in the Pt−PR_3 distances (2.23−2.25 Å) are hardly significant, irrespective of the different basicity and steric hindrance of the P-donor ligands. These findings are in line with the results of a recent QALE analysis of the Rh−P bond lengths for [Rh(CO)(Cl)$(PX_3)_2$] complexes, where it was found that π effects are dominant (53%) over σ electronic and steric factors.[9] Likewise, the Fe−P bond lengths of [Fe(CO)(η-Cp)(COMe)(PX_3)] vary over a narrow range (2.195 ± 0.015 Å) and are only slightly dependent on the σ donicity and size of the ligand.[10] Similar to the Pt−P separations, the N1−Pt−N2 angles also do not change much along the series of determined structures (cf. Table 1).

The introduction of the two methyl substituents, in position 2,9 of the phenanthroline, brings substantial changes to the coordination geometry. The most relevant is a tilt of the dmphen moiety away from the coordination plane, as shown by the values of the dihedral angles between the plane defined by atoms Pt, N1, N2 and that defined by the atoms of the phenanthroline (cf. Table 1) in the range 30−38°. A further effect is the loss of planarity of the ligand as can be seen by the increase of the dihedral angles between the pyridyl moieties (in the range 4−12°). Finally, the coordination plane at the platinum(II) center undergoes a tetrahedral distortion that can be seen from the deviations of atoms P and C1L from the lsq planes defined by the atoms Pt1, N1, N2 and listed in Table 1. All three effects follow the order $PCy_3 > PPh_3 > PPhMe_2 > P(i\text{-}Pr)_3$ that does not reflect a clean steric or electronic character. The same sequence is observed in the decrease of the Pt−N1 separation (i.e., that trans to P atom) (from 2.160(8) to 2.064(7) Å). Surprisingly, the Pt−N1 separation for the P(*i*-Pr)$_3$-containing compound is even shorter than that found in compound **15** containing the unsubstituted phenanthroline (2.101(6) Å).

In contrast, the Pt−N2 separations (i.e., those cis to the PR_3 ligand) show large differences (from 2.149(3) Å in [**8**, R = $PhMe_2$] to 2.205(7) Å in [**14**, R = PCy_3]), depending upon the steric requirements of the cis P-donor ligands. These Pt−N bonds are long, compared with the bonds of 2.02 Å in $[Pt(bpy)_2]^{2+}$ and $[Pt(phen)_2]^{2+}$,[11] showing clearly a strong trans influence of the carbon ligand. Indeed, (cf. Figure 5) the Pt−N2 bond length shows an exponential increase as a

(9) Wilson, M. R.; Prock, A.; Giering, W. P. *Organometallics* **2002**, *21*, 2758−2763.
(10) Liu, H.-Y.; Eriks, K.; Prock, A.; Giering, W. P. *Organometallics* **1990**, *9*, 1758−1756.
(11) (a) Dong, V.; Endres, H.; Keller, H. J.; Moroni, W.; Nöthe, D. *Acta Crystallogr., Sect. B* **1977**, *33*, 2428−2431. (b) Endres, H.; Keller, H. J.; Moroni, W.; Nöthe, D.; Dong, V. *Acta Crystallogr., Sect. B* **1978**, *34*, 1823−1827. (c) Hazell, A.; Mukhopadhyay, A. *Acta Crystallogr., Sect. B* **1980**, *36*, 1647−1649.

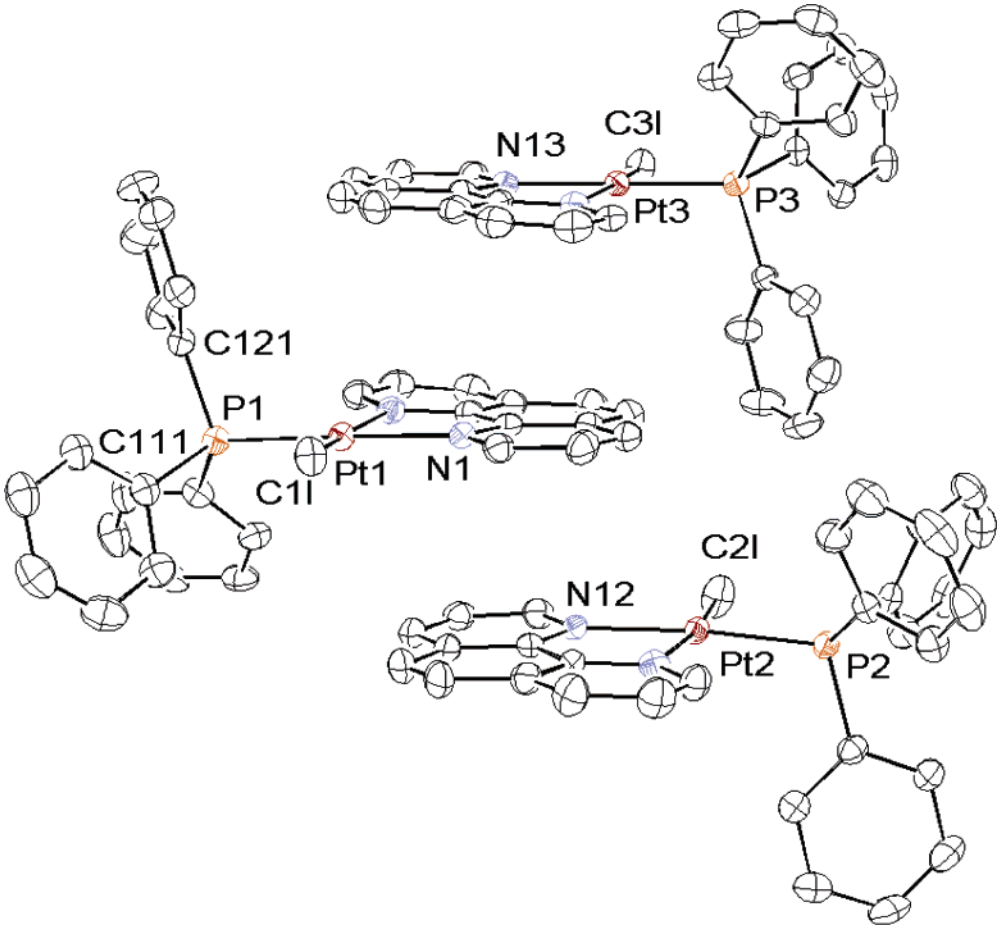

Figure 4. ORTEP view of the cation **15** showing 50% probability ellipsoids.

function of the cone angle of the PR_3 ligand. A similar dependence is obtained by using, instead of the cone angle, an internal steric parameter such as the symmetric deformation coordinate (S_4'') proposed by Orpen et al,[12] (cf. Supporting Information Figure S1). Values of the deformation coordinate for the platinum(II) complexes are reported in Table 1 and are defined by the expression

$$S_4'' = \alpha_1 + \alpha_2 + \alpha_3 - \beta_1 - \beta_2 - \beta_3$$

where α_1, α_2, α_3, and β_1, β_2, β_3 are the C−P−C and P−C−C angles at the coordinate phosphane, respectively. As the steric bulk increases at the coordinate phosphane, S_4'' decreases.

It would seem that the magnitude of phenanthroline distortion, besides the role of the two methyl substituents in position 2,9, is the result of a combined effect of steric and electronic factors induced by opposite P-donor ligands. In particular, an interesting question is to what extent this distortion affects or is affected by the two empty molecular orbitals very close in energy and available to accommodate the extra electrons coming from the electron-rich metal.[13] In contrast, it may be assumed that the observed large deviations from the square-planar geometry are due to the steric hindrance of the phosphane ligand. In addition, to relieve the steric strain, the Pt−N distance cis to the phosphane is stretched and the bond labilized. That is, the steric bulkiness of the PR_3 moiety is accommodated by (a) the lengthening of the Pt−N2 bond and (b) the out-of-coordination plane movement of the P atom (and if necessary of C1L), corresponding to an overall tetrahedral distortion from the square-planar coordination. The largest distortion and the longest Pt−N2 and Pt−P separations are found for the PCy_3-containing compound **14**.

NMR Characterization and Dynamic Behavior of Complexes 1−14. All the proton resonances of compounds **1**−**15** were assigned through NMR spectroscopy from the connectivities in the 2D-NOESY experiments carried out in chloroform-*d* at low temperature. The numbering scheme adopted is shown in Chart 1. Selected ^{1}H NMR data are collected in Table 2, together with the ^{31}P{^{1}H } NMR data.

At 250 K, the ^{1}H NMR spectrum of compound [PtMe(Me$_2$-phen)(PMe$_3$)]BArf **9** in Figure 6, besides the resonances of the aryl groups belonging to the BArf anion (δ = 7.70 and 7.47 ppm) of a methyl group directly coordinated to the metal (δ 0.92, $^2J_{PtH}$ = 72.9 Hz), and of the methyl groups of the PMe_3 ligands (δ 1.46, $^3J_{PtH}$ = 45.2 Hz, $^2J_{PH}$ = 10.5 Hz), shows two singlets, one for each methyl (at δ = 2.97 and 2.91, respectively), four doublets for H_4 (δ 8.31), H_7 (δ 8.25), H_3 (δ 7.64), and H_8 (δ 7.57) protons, and an

(12) Dunne, B. J.; Morris, R. B.; Orpen, A. G. *J. Chem. Soc., Dalton Trans.* **1991**, 653−661.
(13) Klein, A.; Kaim, W.; Waldhör, E.; Hausen, H. D. *J. Chem. Soc., Perkin Trans. 2* **1995**, 2121−2126.

Table 1. Selected Bond Distances (Å) and Angles (deg) for Compounds **1**, **8**, **11**, **14**, **15**

	PPh_3 **1**	$PPhMe_2$ **8**	$P(i\text{-}Pr)_3$ **11**	PCy_3 **14**	PPh_3 **15**[a]
			Bond Distances		
Pt−P1	2.233(8)	2.225(3)	2.232(2)	2.247(2)	2.224(3)
Pt−N1	2.152(3)	2.131(2)	2.064(7)	2.160(8)	2.101(6)
Pt−N2	2.162(3)	2.149(3)	2.184(7)	2.205(7)	2.14(1)
Pt−C11	2.052(4)	2.124(3)	2.03(2)	2.01(1)	2.041(6)
			Angles		
C11−Pt−N1	95.5(1)	94.4(1)	87.6(8)	93.7(4)	92.4(8)
C11−Pt−N2	171.4(1)	171.2(1)	163.5(8)	169.6(4)	170.8(9)
N1−Pt−N2	76.4(1)	77.5(1)	78.0(3)	76.0(3)	78.7(2)
C11−Pt−P1	86.2(1)	83.94(9)	85.1(8)	87.6(3)	89.1(6)
N1−Pt−P1	165.13(7)	170.74(7)	171.3(2)	159.5(2)	177(2)
N2−Pt−P1	100.92(7)	103.64(8)	108.6(2)	102.6(2)	99.8(6)
Pt−P1−C111−C112	134.1(3)	132.6(3)	166.6(9)	166.6(6)	111.3(4), 126.1(3), 145.2(3)
			Angles between lsq Planes		
C10′−C6′−C6−C5−C4′−C10 ∧ N1−C2−C3−C4 −C4′	9.6(2)	8.95(2)	4(1)	11.2(4)	0.7(8)
C10′−C6′−C6−C5−C4′−C10 ∧ N2−C9−C8−C7−C6′−C10′	8.7(2)	9.01(2)	8(1)	12.2(4)	1.0(8)
dmphen[b] ∧ N1−Pt−N2	36.2(1)	33.8(1)	29.7(3)	38.6(2)	4.01(9)
Δd(P1), Δ*d*(C1l)[c]	0.57, 0.10	−0.35, −0.12	0.22, 0.29	0.79, −0.06	−0.08, 0.09
deformation coordinate (S_4'')[d]	29.5	33.5	27.8	25.4	24.2

[a] Average values; for the torsion angles the values for the three independent molecules in the asymmetric unit are listed. ESDs on the average are obtained from the formula: $\sigma^2 = \sum(x_i - \bar{x})/(N-1)$ where N = number of observations. [b] dmphen refers to the lsq plane defined by the atoms of the phenanthroline moiety, except the two carbons in positions 2,9. [c] Δ*d*(P1), Δ*d*(C1l) are the deviations (Å) of atoms P1 and C1l, from the lsq plane defined by the atoms Pt, N1, N2, respectively (ESDs ≤ 0.02 Å). [d] For the definition see text.

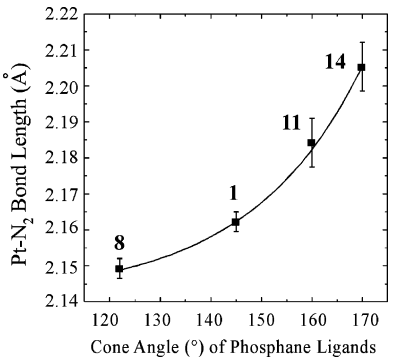

Figure 5. Increase of the Pt−N2 bond separation with increasing cone angle of the coordinated phosphanes.

Chart 1. Structural Formula of Complexes with Atomic Numbering

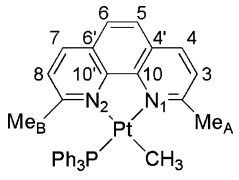

AB system for H_5 (δ 7.75) and H_6 (δ 7.72) protons as a result of the asymmetry of a firmly bonded bidentate phenanthroline.

At a higher temperature (319 K), the two methyl groups and the aromatic proton pairs H_3-H_8, H_4-H_7, and H_5-H_6 become chemically equivalent, indicating a fast site exchange of proton sites, which is required by interchange of the two nitrogen atoms of the Me_2-phen ligand. The main features of the ^{1}H NMR phenanthroline peaks for the complex [Pt(Me)(Me_2-phen)($P(4\text{-}ClC_6H_4)_3$]]BArf, **3** (Figure 7) are essentially similar to those of compound **9** except for the resonance of the methyl proton Me_B that is consistently shifted to lower frequencies (at δ 1.95) as a result of ring current from phenyl substituents on the arylphosphane bound in the cis position. As can be seen from the data in Table 2, a wider difference of chemical shift between the Me_A and Me_B groups of protons characterizes the ^{1}H NMR spectra of the complexes containing arylphosphanes (**1**−**6**) or mixed alkyl−arylphosphanes (**7**, **8**, **12**, **13**) with respect to those of compounds with alkylphosphanes (**9**−**11**, **14**).

The passage from slow to fast exchange was followed either through the ^{1}H NMR spectral changes of the aromatic proton pair H_4-H_7 or from those of the Me_2-phen methyl groups. The process is clearly intramolecular. A lack of exchange has been shown previously[1] by a deliberate addition of Me_2-phen to a solution of **1** in $CDCl_3$. In addition, for all the examined systems **1**−**14** and at any temperature, there was no indication of the presence of free phenanthroline in solution. Unfortunately, the coupling constants of the protons of Me_2-phen with ^{195}Pt were too weak to be observed. However, the coupling constants of the coordinated methyl protons and of the phosphorus atom (see Table 2) are retained, showing values typical of methyl and phosphane groups in the position trans to nitrogen atoms. The rate constants for the flipping of complexes **1**−**14** at different temperatures were determined by a full line-shape analysis (Supporting Information Table S1).

The activation parameters for the fluxional process were derived from Eyring plots and are listed in Supporting Information Table S2. In Table 3 are reported the values of the rates (at 340 K) and of the activation energies for the flipping of Me_2-phen, together with the values of the stereoelectronic parameters of the P-donor ligands. Overlapping of the monitored peaks with other ligand peaks for the $PCy_2(C_6H_5)$-containing compound **13** prevented a satisfactory line-shape analysis of the temperature dependence of the NMR spectra that resulted in a poor correspondence between experimental and simulated spectra.

Discussion

The nature of the P-donor ligands L markedly affects the rates of fluxional motion of Me_2-phen as well as the values of the $^1J_{PtP}$ coupling constants of the [Pt(Me)(PR_3)(Me_2-phen)]TFBP complexes (cf. data in Table 3). The efficiency of the spectator P-donor ligands in accelerating the rearrangement increases in the order $P(4\text{-}MeC_6H_4)_3 < P(4\text{-}MeOC_6H_4)_3 < PCy(C_6H_5)_2 < P(C_6H_5)_3 < P(4\text{-}FC_6H_4)_3 < PMe(C_6H_5)_2 < P(4\text{-}ClC_6H_4)_3 < PMe_2(C_6H_5) < P(4\text{-}CF_3C_6H_4)_3 < PEt_3 < PMe_3 < P(i\text{-}Pr)_3 < PCy_3$, the difference in reactivity between the first and the last members of the series being 2 orders of magnitude. The entropy changes $\Delta S^{\ddagger}$ range in magnitude from −80 to +35 J K^{-1} mol^{-1} (see data in Supporting Information Table S2), but these values must be considered with some caution and cannot provide any real insight into the nature of the fluxional process because of their extreme sensitivity to systematic errors associated with

Table 2. Selected ^{1}H and ^{31}P{^{1}H} NMR Data for the Platinum(II) Complexes [Pt(Me)(Me$_2$-phen)(P)]BArf **1**−**15**[a]

		δ^1H						δ^{31}P
	phosphane (P)	H_4	H_7	Me_A	Me_B	CH_3-Pt	others	
1	$P(C_6H_5)_3$	8.32	8.15	3.02	1.90	0.74 (66.9)	7.52 ($H_{o,o'}$-P)	14.3 (4575)
2	$P(4\text{-}FC_6H_4)_3$	8.32	8.21	2.99	1.92	0.69 (74.0)	7.51 ($H_{o,o'}$-P)	12.3 (4618)
3	$P(4\text{-}ClC_6H_4)_3$	8.33	8.26	3.00	1.95	0.69 (74.4)	7.40 ($H_{o,o'}$-P)	13.2 (4622)
4	$P(4\text{-}CF_3C_6H_4)_3$	8.27	8.18	2.97	1.86	0.73 (70.0)	7.69 ($H_{o,o'}$-P)	15.1 (4656)
5	$P(4\text{-}MeOC_6H_4)_3$	8.32	8.18	3.02	2.02	0.75 (75.2)	7.46 ($H_{o,o'}$-P); 3.81 (O-CH_3)	9.8 (4561)
6	$P(4\text{-}MeC_6H_4)_3$	8.33	8.15	3.02	1.95	0.73 (74.5)	7.41 ($H_{o,o'}$-P); 2.37 (P-CH_3)	12.0 (4557)
7	$PMe(C_6H_5)_2$	8.30	8.10	3.02	1.97	0.90 (72.5)	1.94 ($^3J_{PtH}$ = 52.7, P-CH_3)	−1.0 (4534)
8	$PMe_2(C_6H_5)$	8.31	8.13	3.02	2.13	1.00 (74.2)	1.76 ($^3J_{PtH}$ = 47.4, P-CH_3)	−18.1 (4379)
9	PMe_3	8.31	8.25	2.97	2.91	0.92 (72.9)	1.46 ($^3J_{PtH}$ = 45.2, P-CH_3)	−31.8 (4291)
10	PEt_3	8.25	8.18	2.95	2.91	0.84 (72.5)	1.72 (P-CH_2CH_3), 0.87 (P-CH_2CH_3)	3.4 (4327)
11	$P(i\text{-}Pr)_3$	8.23	8.22	2.94	2.92	0.96 (73.8)	2.32 (P-$CHCH_3$), 1.04 (P-$CHCH_3$)	23.9 (4358)
12	$PCy(C_6H_5)_2$	8.29	8.18	2.98	2.01	0.95 (70.3)	2.62, (P-CH); 1.91, 1.62 1.25, 0.88 (C-CH_2)	13.7 (4501)
13	$PCy_2(C_6H_5)$	8.33	8.22	3.03	1.85	1.03 (72.9)	2.48 (P-CH); 1.98−1.54, 1.47−1.05 (C-CH_2)	11.8 (4287)
14	PCy_3	8.29	8.25	3.00	2.93	0.93 (74.6)	2.09 (P-CH); 1.68, 1.42, 1.14 (C-CH_2)	13.0 (4315)
15	$P(C_6H_5)_3$[b]	8.88	8.68			0.92 (69.8)	9.33 ($^3J_{PtH}$ = 35.2, H_2), 7.80 ($H_{o,o'}$-P), 7.69 ($^3J_{PtH}$ = 17.0, H_9)	19.1 (4395)

[a] Recorded in $CDCl_3$ as solvent at appropriate temperature (see Experimental Section). Chemical shifts (δ) are in ppm and coupling constants, $^2J_{PtH}$ for ^{1}H and $^1J_{PtP}$ for ^{31}P given in parentheses, are in hertz. [b] Compound containing unsubstituted 1,10-phenanthroline.

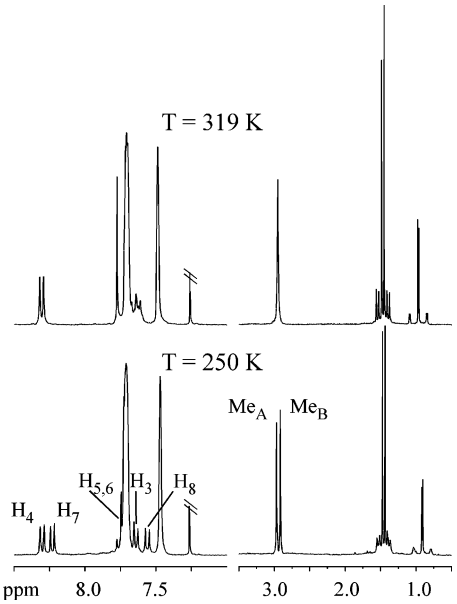

Figure 6. Section of the ^{1}H NMR spectrum of complex **9** recorded at 300.13 MHz in chloroform-*d* at 250 K (lower plot) and at 319 K (upper plot).

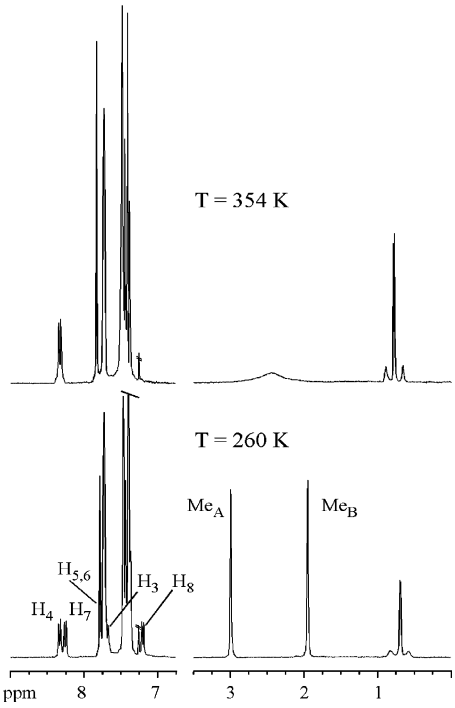

Figure 7. Section of the ^{1}H NMR spectrum of complex **3** recorded at 300.13 MHz in chloroform-*d* at 260 K (lower plot) and at 354 K (upper plot).

the line-shape analysis. The activation energies $\Delta G^{\ddagger}$ (340 K) are more meaningful.[14]

Quantitative Separation of Electronic and Steric Effects. To correlate electronic or steric effects of the P-donor ligands with any physicochemical property of the system, it is necessary to dissect the overall effect into its steric and electronic components. A general and quantitative approach to the problem (QALE) has been developed over the last 20 years, particularly by groups of Giering and Prock and Poë[15] and has been applied to a large body of kinetic, thermodynamic, NMR, spectroscopic, and structural data.[16] Appropriate parameters for P-donor ligands are Bartik's infrared parameter χ, which describes the σ-electron donor capacity of the ligands (a small χ value is associated with a good σ donation),[17,18] and Tolman's cone angle θ, which measures the steric requirements as derived from space-filling CPK molecular models of the ligands.[19] Variants of the cone angle concept have been suggested on the basis of math-

(14) Sandström, J. *Dynamic NMR Spectroscopy*; Academic Press: London, 1982; ISBN 0-12-618620.

(15) A complete list of references can be found in the recent papers (a) Woska, D.; Prock, A.; Giering, W. P. *Organometallics* **2000**, *19*, 4629−4638. (b) Fernandez, A.; Reyes, C.; Lee, T. Y.; Prock, A.; Giering, W. P.; Haar, C. M.; Nolan, S. P. *J. Chem. Soc., Perkin Trans.* **2000**, *2*, 1349−1357. (c) Fernandez, A. L.; Reyes, C.; Prock, A.; Giering, W. P. *J. Chem. Soc., Perkin Trans.* **2000**, *2*, 1033−1041. (d) Babij, C.; Che, H.; Chen, L.; Poë, A. J. *J. Chem. Soc., Dalton Trans.* **2003**, 3184−3191. (e) Bunten, K. A.; Chen, L.; Fernandez, A. L.; Poë, A. J. *J. Coord. Chem. Rev.* **2002**, *233*−*234*, 41−51. (f) Poë, A. J.; Moreno, C. *Organometallics* **1999**, *18*, 5518−5530.

(16) http://www.bu.edu/qale. This Web site collects sets of data, protocol for the analysis, program package, parameters of ligands, leading references, etc. Each set of data, taken from the literature, is subjected to a QALE analysis with commentary on how each analysis is done and how successful it is. All the material is updated with recent data sets and analyses.

Table 3. Selected Kinetic and NMR Data for [Pt(Me)(Me_2-phen)(P)]BArf **1**−**14** Complexes and Stereoelectronic Parameters of the Corresponding P-Donor Ligands

	phosphane	χ^a cm^{-1}	θ^a deg	$E_{ar}{}^a$	$^1J_{PtP(exp)}{}^b$ Hz	$^1J_{PtP(calc)}{}^c$ Hz	$k_{f(340)}{}^d$ s^{-1}	$\Delta G_{(exp)}{}^{\ddagger e}$ kJ mol^{-1}	$\Delta G_{(calc)}{}^{\ddagger f}$ kJ mol^{-1}
1	$P(C_6H_5)_3$[e]	13.25	145	2.7	4575	4585	119	70.1	69.8
2	$P(4\text{-}FC_6H_4)_3$	15.7	145	2.7	4618	4610	176	69.0	68.8
3	$P(4\text{-}ClC_6H_4)_3$	16.8	145	2.7	4622	4621	258	67.9	68.3
4	$P(4\text{-}CF_3C_6H_4)_3$	20.5	145	2.7	4656	4659	348	66.9	66.7
5	$P(4\text{-}MeOC_6H_4)_3$	10.5	145	2.7	4561	4556	93.7	70.8	71.0
6	$P(4\text{-}MeC_6H_4)_3$	11.5	145	2.7	4557	4567	86.5	71.0	70.6
7	$PMe(C_6H_5)_2$	12.6	136	2.2	4534	4517	211	68.5	69.1
8	$PMe_2(C_6H_5)$	10.5	122	1	4379	4381	292	67.6	67.4
9	PMe_3	8.55	118	0	4291	4294	493	66.1	66.0
10	PEt_3	6.3	132	0	4327	4326	385	66.8	66.8
11	$P(i\text{-}Pr)_3$	3.45	160	0	4358	4353	2018	62.1	62.1
12	$PCy(C_6H_5)_2$	9.1	153	1.6	4501	4503	108	70.4	68.0[g]
13	$PCy_2(C_6H_5)$	5.7	162	1.6	4287	4452[g]			
14	PCy_3	1.4	170	0	4315	4316	8029	58.2	58.1

[a] From http://www.bu.edu/quale/. [b] Values of experimental $^1J_{PtP}$ coupling constants for complexes **1**−**14**. [c] Values of $^1J_{PtP}$ coupling constants calculated from QALE analysis. [d] Rates of the fluxional motion of Me_2-phen in the complexes **1**−**14** at 340 K. [e] Activation energies for the flipping at 340 K. [f] Activation energies derived from QALE analysis. [g] Deviant data treated as outliers in the QALE analysis.

ematical models,[20] X-ray structural data,[21] or upon molecular mechanics calculations.[22] However, their use does not necessarily improve the data analysis.[15e] The concepts of sharp steric thresholds θ_{st} (below which no steric effects are evident)[23] and the so-called aryl effect E_{ar} (which depends on the number of aryl groups)[24] were introduced, as well as, more recently, π-acidity (π_p) effects[15a,b] and an extension of an apparent aryl effect to ligands that do not actually contain aryl groups attached to the P-donor atoms.[15c] In addition, the stereoelectronic parameters for P-donor ligands (χ, θ, E_{ar}) are transferable to other groups of ligands, including silyl,[25] arsines, nitriles,[26] amines, thioethers,[27] and sulfoxides.[2]

Equation 2 is a general form of the QALE equation for ligands having no π-acidity (π_p) effects and systems that might contain up to one observable steric threshold:

$$\text{property} = \omega + \alpha(\chi) + \beta(\theta) + \beta'(\theta - \theta_{st})\lambda + \gamma(E_{ar}) \quad (2)$$

where χ, θ, θ_{st}, and E_{ar} have the meaning illustrated above, λ is a switching function that equals 0 when $\theta < \theta_{st}$ and equals 1 when $\theta > \theta_{st}$. α, β, β', and γ are regression coefficients that measure the relative importance of electronic, steric, and aryl factors in the process. The response of the property to χ is assumed to be *linear* over the entire range of ligands, while the response to the steric parameter ($\theta - \theta_{st}$) is not linear. Equation 2 allows for nonzero steric effects below the steric threshold (the $\beta(\theta)$ term) with a different steric effect above the steric threshold (the $\beta'(\theta - \theta_{st})$ term). If there is no observable steric threshold, then the "$\beta'(\theta - \theta_{st})$" term is set to zero. The presence of so many variables makes the results from regression analysis questionable, especially in the detection of a meaningful value for the steric threshold. Keeping in mind this difficulty, very recently Giering, Prock et al.[28] proposed a combined method of graphical and regression analysis of ligand effect data, based essentially on the use of data obtained from graphical analysis to control the results of the regression analysis. This protocol has been applied to the NMR and kinetic data in Table 3.

"Graphical" Analysis of the Kinetic Data. A good estimate of α can be obtained from the plot of $\Delta G^{\ddagger}$ vs χ for the isosteric $P(p\text{-}XC_6H_4)_3$ ligands as shown in Figure 8.

Since the parameters $\theta = 145°$ and $E_{ar} = 2.7$ are both constant for this ligand set (compounds **1**−**6**), the variation in the $\Delta G^{\ddagger}$ values should reflect the sensitivity of the system to ligand σ basicity only. In practice, the slope of this plot ($\alpha = -0.435 \pm 0.04$ kJ mol^{-1} cm, $r^2 = 0.981$, 6 data points) affords a fast estimate of the coefficient of χ for the full set of data in the QALE equation. There is an inhibitory electronic effect on the rates since the activation energy for the fluxional motion of Me_2-phen is enhanced as the phosphanes become better electron donors (smaller χ). The

(17) Bartik, T.; Himmler, T.; Schulte, H. G.; Seevogel, K. *J. Organomet. Chem.* **1984**, *272*, 29−41.

(18) A value of χ for a ligand L is obtained from the difference between the A_1 carbonyl stretching frequency (ν_{CO} in units of cm^{-1}) for $LNi(CO)_3$ and the constant value, 2056.1 cm^{-1}.

(19) Tolman, C. A. *Chem. Rev.* **1977**, *77*, 313−348.

(20) (a) Seligson, A. L.; Trogler, W. C. *J. Am. Chem. Soc.* **1991**, *113*, 2520−2527. (b) Imyatov, N. S. *Koord. Khim.* **1985**, *11*, 1041, 1171−1178.

(21) (a) Alyea, E. C.; Dias, S. A.; Ferguson, G.; Restivo, R. J. *Inorg. Chem.* **1977**, *16*, 2329−2334. (b) Ferguson, G.; Roberts, P. J.; Alyea, E. C.; Khan, M. *Inorg. Chem.* **1978**, *17*, 2965−2967. (c) Alyea, E. C.; Dias, S. A.; Ferguson, G.; Parvez, M. *Inorg. Chim. Acta* **1979**, *37*, 45−52. (d) Immirzi, A.; Musco, A. *Inorg. Chim. Acta* **1977**, *25*, L41−L42. (e) Porzio, W.; Musco, A.; Immirzi, A. *Inorg. Chem.* **1980**, *19*, 2537−2540. (f) Müller, T. E.; Mingos, D. M. P. *Transition Met. Chem.* **1995**, *20*, 533−539. (g) Smith, J. M.; Coville, N. J. *Organometallics* **2001**, *20*, 1210−1215. (h) Smith, J. M.; Coville, N. J.; Cooke, L. M.; Boeyens, J. C. A. *Organometallics* **2000**, *19*, 5273−5280.

(22) (a) Caffrey, M. L.; Brown, T. L. *Inorg. Chem.* **1991**, *30*, 3907−3914. (b) Brown, T. L. *Inorg. Chem.* **1992**, *31*, 1286−1294. (c) Brown, T. L.; Lee, K. J. *Coord. Chem. Rev.* **1993**, *128*, 89−116. (d) Choi, M. G.; Brown, T. L. *Inorg. Chem.* **1993**, *32*, 1548−1553.

(23) Liu, H.-Y.; Eriks, K.; Prock, A.; Giering, W. P. *Organometallics* **1990**, *9*, 1758−1766.

(24) (a) Wilson, M. R.; Woska, D. C.; Prock, A.; Giering, W. P. *Organometallics* **1993**, *12*, 1742−1752. (b) Farrar, D. H.; Hao, J.; Poë, A. J.; Stromnova, T. A. *Organometallics* **1997**, *16*, 2827−2832.

(25) (a) Panek, J.; Prock, A.; Eriks, K.; Giering, W. P. *Organometallics* **1990**, *9*, 2175−2176. (b) Lorsbach, B. A.; Prock, A.; Giering, W. P. *Organometallics* **1995**, *14*, 1694−1699.

(26) Fernandez, A. L.; Prock, A.; Giering, W. P. *Organometallics* **1994**, *13*, 2767−2772.

(27) (a) Tracey, A. A.; Eriks, K.; Prock, A.; Giering, W. P. *Organometallics* **1990**, *9*, 1399−1405. (b) Fernandez, A. L.; Prock, A.; Giering, W. P. *Organometallics* **1996**, *15*, 2784−2789.

(28) Bartholomew, J.; Fernandez, A. L.; Lorsbach, B. A.; Wilson, M. R.; Prock, A.; Giering, W. P. *Organometallics* **1996**, *15*, 295−301.

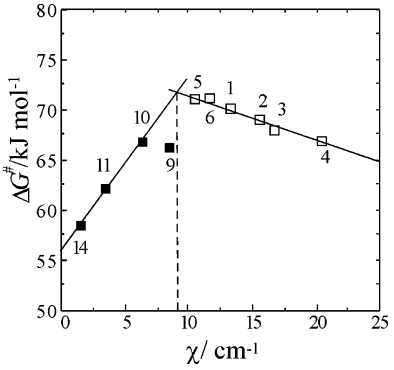

Figure 8. Plot of $\Delta G^{\ddagger}$ vs χ for isosteric triaryl P-donor ligands (**1**−**6**, empty squares) and trialkyl P-donor ligands (**9**−**11**, **14**, filled squares).

data for three of the trialkyl phosphanes **10**, **11**, **14** fit a reasonably good straight line with a positive slope that intersects the previous line at a value of χ close to 8.2. These observations allow for two main conclusions to be drawn: (i) there is a dominant steric effect associated with the trialkyl P-donor ligands that operates in opposite direction to the σ-donor effect (otherwise the two sets of data would lie on the same line), and (ii) there is a significant aryl effect. In the absence of an aryl effect, the two lines would have intersected at a value of $\chi = 4.7$, corresponding to the basicity of an hypothetical trialkyl ligand with a cone angle of 145°, the same as those of the triarylphosphanes. The magnitude of the deviation is a measure of the aryl effect. The experimental line for the triarylphosphanes (**1**−**6**) lies almost 6 kJ mol^{-1} above a parallel imaginary line intersecting the trialkylphosphane line at $\chi = 4.7$, which suggests that the aryl effect operates in the same direction as the electron σ donation, increasing $\Delta G^{\ddagger}$ and leading to a pronounced decrease in the rates. Since the value of $E_{ar} = 2.7$ for the triarylphosphanes, the value expected for γ in eq 2 is 6/2.7 = 2.22 kJ mol^{-1}.

In the search for a steric threshold, we found that a plot of $\Delta G^{\ddagger}$ vs "*i*" (where "*i*" represents the number of aryl groups of a component of the family of the mixed alkyl−arylphosphane) was perfectly linear (slope = 1.29 ± 0.09 kJ mol^{-1}, $r^2 = 0.995$, 4 data points), thus suggesting the absence of a steric threshold at least until the value of the cone angle of the most sterically hindered ligand (PPh_3, $\theta = 145°$). However, the steric profile constructed on plotting the values of $\Delta G^{\ddagger}$ vs θ for the alkyl phosphanes (**9**−**11**, **14**) suggested the presence of a steric threshold in the cone angle range of 147−149°.

Regression Analysis of the Kinetic Data. A regression analysis provides a more accurate evaluation of the single contributions of the stereoelectronic parameters to the activation energy of the Me_2-phen flipping. The graphical analysis suggests that eq 2 is suitable to analyze the energy data in Table 3 since it accounts for steric (θ) and electronic ($\sigma + E_{ar}$) effects as well as for the presence of a steric threshold. The results of the first regression analysis of all data points ($n = 13$), performed using eq 2 and the SCIENTIST program,[29] revealed that $PCy(C_6H_5)_2$ must be considered an outlier. The exclusion of $PCy(C_6H_5)_2$ increased significantly the quality of the fit, but it appeared that the contribution of the parameter β was statistically insignificant. Accordingly, it was dropped from the analysis, and the datum for $PCy(C_6H_5)_2$ was removed from the data set. The resulting regression equation is

$$\Delta G^{\ddagger} = (70.6 \pm 3) + (-0.43 \pm 0.04)(\chi) - (0.47 \pm 0.05)(\theta - 148°)\lambda + (2.2 \pm 0.3)(E_{ar})$$

(data points = 12, DC = 0.997, MSC = 4.27) (3)

that corresponds to steric and electronic contributions of 38 and 40%, respectively, and of about 22% for the aryl contribution.[30] As a measure of goodness-of-fit, we use the coefficient of determination DC = 0.997 and the value of MSC = 4.918 (model selection criterion).[31] An appropriate index of goodness-of-fit is also given by the correspondence between the values of α (−0.425 ± 0.04 kJ mol^{-1} cm) obtained from full regression analysis and the value of α (−0.435 ± 0.04 kJ mol^{-1} cm) obtained from the plot of $\Delta G^{\ddagger}$ vs χ for the isosteric ligands $P(4\text{-}XC_6H_4)_3$, where θ and E_{ar} remain constant (Figure 8). There is also an excellent correspondence between the values of γ from full regression ($\gamma = 2.23 \pm 0.3$ kJ mol^{-1}) and the value resulting from the graphical analysis ($\gamma = 2.22$ kJ mol^{-1}). The values of $\Delta G^{\ddagger}$ calculated using the regression coefficients in eq 3 are included in Table 3. A significant deviation from the experimental data is observed only for $PCy(C_6H_5)_2$, which we have treated as an "outlier".

Stereoelectronic Analysis of $^1J_{PtP}$ Coupling Constants. The values of $^1J_{PtP}$ coupling constants of the complexes **1**−**14** in Table 3 were analyzed with eq 2, setting apart the value for complex **13** and using the values of χ, θ, and E_{ar} as stereoelectronic parameters of the ligands. The QALE analysis has been performed according to the protocol described above for the kinetic data and led to the equation:

$$^1J_{PtP} = (3745 \pm 54) + (10.3 \pm 1)(\chi) + (3.9 \pm 0.4)(\theta) + (-5.5 \pm 1)(\theta - 150)\lambda + (51 \pm 5)(E_{ar})$$

(data points = 13, DC = 0.997, MSC = 5.07) (4)

At variance with the results of the analysis performed on the kinetic data, for the NMR data the $\beta(\theta)$ term of eq 2 is statistically significant, indicating that there is a nonzero positive steric effect below the steric threshold. The values of $^1J_{PtP}$ calculated using the regression coefficients in eq 4 are included in Table 3. A significant deviation from the

(29) *SCIENTIST*; Micro Math Scientific Software: Salt Lake City, UT.

(30) A useful way to display the extent to which a parameter affects a property is to calculate the percentage contribution of that parameter using the regression coefficients derived from eq 3 and defining the maximum range of variation of the parameters ($\Delta\chi = 26$ cm^{-1}; $\Delta\theta = 22°$; $\Delta E_{ar} = 2.7$), according to the equation: $\%\chi = 100(|\alpha|\ \Delta\chi)/[(|\alpha|\ \Delta\chi) + (|\beta|\ \Delta\theta) + (|\gamma|\Delta E_{ar})]$.

(31) The coefficient of determination DC measures the fraction of the total variance accounted for by the model. When dealing with a multiplicity of possible models, a more appropriate index of goodness-of-fit is the MSC (model selection criterion). The most appropriate model will be that with the largest MSC. A supplementary statistical criterion is given by the value of $r^2 = 0.994$ for the linear plot of $\Delta G^{\ddagger}_{(calc)}$ vs $\Delta G^{\ddagger}_{(obs)}$, where $\Delta G^{\ddagger}_{(calc)}$ is obtained by introducing the calculated coefficients in eq 3.

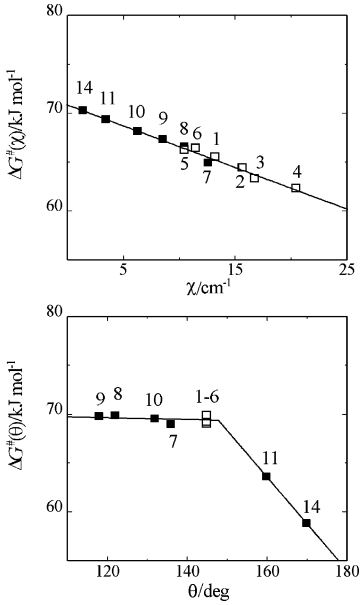

Figure 9. Electronic profile (upper plot) and steric profile (lower plot) for the free activation energy of the fluxional motion of Me_2-phen in $[PtMe(Me_2\text{-phen})(PR_3)]^+$. Open squares refer to complexes containing triaryl P(4-$XC_6H_4)_3$ phosphanes.

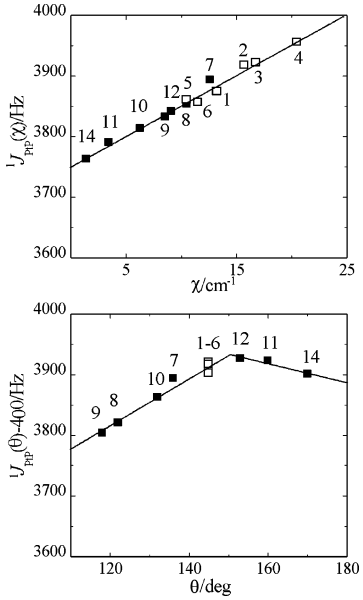

Figure 10. Electronic profile (upper plot) and steric profile (lower plot) for the $^1J_{PtP}$ values of $[PtMe(Me_2\text{-phen})(PR_3)]^+$ complexes.

experimental data is observed only for $PCy_2(C_6H_5)$, which we have considered as an "outlier" in the QALE analysis.

Stereolectronic Profiles. The results of the QALE analysis can now be displayed as electronic, steric, and E_{ar} profiles (Figures 9 and 10).

These plots were constructed by subtracting from the experimental data the contributions of all the terms of the regression eqs 3 and 4, except that of the variable of interest, (i.e., $\alpha(\chi)$ in the electronic profiles).[32] For the sake of space, the aryl profiles are omitted in Figures 9 and 10, but it is of interest to reiterate that the aryl effect has a significant positive effect on both the properties analyzed (the regression coefficients $\gamma(E_{ar})$ are both positive 2.23 kJ mol^{-1} and 50.5 Hz for $\Delta G^{\ddagger}$ and $^1J_{PtP}$, respectively). The electronic profile in Figure 9A indicates that the activation energy for the fluxional motion of Me_2-phen in the complexes is enhanced as the phosphanes become better electron donors (smaller χ, $\alpha = -0.425 \pm 0.04$ kJ mol^{-1} cm).

In contrast, the values of $^1J_{PtP}$ coupling constants decrease linearly with increasing electron donation by the P-donor ligands, as indicated by the electronic profile in Figure 10A. The two steric profiles exhibit well-defined steric thresholds at 150° for $^1J_{PtP}$ (Figure 10B) and at 148° for $\Delta G^{\ddagger}$ (Figure 9B), the only difference being that along the set of small ligands (characterized by values of cone angle $\theta < \theta_{st}$), the coupling constants $^1J_{PtP}$ increase before the onset of the steric threshold, while the same set of ligands does not affect significantly the activation energy $\Delta G^{\ddagger}$ of the flipping.

Bonding of Phosphanes to Platinum by NMR. Coupling constants $^1J_{PtP}$ of closely related planar platinum(II) complexes can be regarded as a good diagnostic probe of the changes in 6s character of the hybrid orbital of platinum used in bonding to the phosphorus atom.[33] Smaller values of $^1J_{PtP}$ correspond to longer Pt−P bond distances and to higher trans influences of groups in trans position to the bond.[34] We have summarized in Table 4 the results of the QALE analysis carried out on $^1J_{PtP}$ of complexes **1**−**14** (coefficients and statistics), together with similar regression analysis of data for other platinum(II) complexes taken from the recent literature.

The value of α (10.3 ± 1 Hz cm), which represents the sensitivity of $^1J_{PtP}$ of $[Pt(Me)(Me_2\text{-phen})(PR_3)]^+$ to the inductive effects brought about by substituents on phosphorus, is comparable to that of other cationic complexes having the same N−Pt−P bond axis as that for $[Pt(N{-}N{-}C)(PR_3)]^+$ (N−N−CH = 6-(1-methylbenzyl)-2.2′-bipyridine, $\alpha = 14.1 \pm 3$ Hz cm),[35] or the same P−Pt−P bond axis as that for *trans*-$[Pt(PR_3)_2Me(CH_3OH)]^+$[36] ($\alpha = 14.6 \pm 2$ Hz cm) and *trans*-$[Pt(PR_3)_2MeCl]$[37] ($\alpha = 11.3 \pm 0.5$ Hz cm). In contrast, for uncharged complexes of cis geometry having either strong or weak trans-activating groups, $^1J_{PtP}$ increases on increasing the electron-donor ability of the substituent on the phosphorus ligand. The values of α (Hz cm) are -8.5 ± 0.7 for *cis*-$[PtPh_2(CO)(PR_3)]$,[38] -6 ± 1 for *cis*-$[PtMe_2(PR_3)_2]$,[36] -7.2 ± 0.8 for *cis*-$[PtMe_2(PR_3)(Me_2SO)]$,[39] -8.1 ± 0.9 for *cis*-$[PtMe_2(PR_3)(py)]$,[39] and -8.9 ± 0.3 for *cis*-$[Pt(PR_3)_2Cl_2]$.[37] For *cis*-$[Pt(PR_3)_2MeCl]$,[37] α is -3.4 ± 0.3 with PR_3 trans to

(32) As an example, the electronic profile in the upper plot of Figure 9 was constructed according to the equation $\Delta G^{\ddagger}(\chi) = \Delta G^{\ddagger}_{(obsd)} - (\beta'\text{-}(\theta - \theta_{st})\lambda + \gamma(E_{ar}))$.

(33) Allen, F. H.; Pidcock, A. *J. Chem. Soc. A* **1968**, 2700−2704.
(34) (a) Appleton, T. G.; Clark, H. C.; Manzer, L. E. *Coord. Chem. Rev.* **1973**, *10*, 335−422. (b) Appleton, T. G.; Bennett, M. A. *Inorg. Chem.* **1978**, *17*, 738−747. (c) Grim, S. O.; Keiter, R. L.; McFarlane, W. *Inorg. Chem.* **1967**, *6*, 1133−1137. (d) Allen, F. H.; Sze, S. N. *J. Chem. Soc. A* **1971**, 2054−2056.
(35) Romeo, R.; Plutino, M. R.; Monsù Scolaro, L.; Stoccoro, S. *Inorg. Chim. Acta* **1997**, *265*, 225−233.
(36) Romeo, R.; Alibrandi, G. *Inorg. Chem.* **1997**, *36*, 4822−4830.
(37) Cobley, C. J.; Pringle, P. *Inorg. Chim. Acta* **1997**, *265*, 107−115.
(38) Romeo, R.; Arena, G.; Monsù Scolaro, L. *Inorg. Chem* **1994**, *33*, 4029−4037.
(39) Romeo, R.; Monsù Scolaro, L.; Plutino, M. R.; Fabrizi de Biani, F.; Bottari, G.; Romeo, A. *Inorg. Chim. Acta* **2003**, *350*, 143−151.

Table 4. Selected Coefficients Derived from QALE Analysis for $^1J_{PtP}$ of Some Platinum(II) Complexes

complexes	n[a]	α Hz cm	β Hz deg^{-1}	β' Hz deg^{-1}	γ Hz	ω Hz	θ_{st} deg	DC[b]	MSC[c]	ref
$[Pt(Me)(dmphen)(PR_3)]^+$	13	10.3± 1	3.91 ± 0.4	−5.5 ± 1	51 ± 6	3745 ± 54	150	0.997	5.07	this work
$[Pt(N-N-C)(PR_3)]^+$	14	14.1 ± 3	4.1 ± 0.6		43 ± 10	3515 ± 90	<122	0.975	3.11	35
trans-$[Pt(Me)(PR_3)_2(MeOH)]^+$	13	14.6 ± 2	3.6 ± 0.6	−3.7 ± 1	64 ± 7	2240 ± 62	151	0.997	4.98	36
trans-$[PtMeCl(PR_3)_2]$[d]	6	11.3 ± 0.5				2989 ± 7		0.993	4.30	37
cis-$[Pt(Ph)_2(CO)(PR_3)]$	10	−8.5 ± 0.7	−4.9 ± 0.3			2480 ± 50	<122	0.973	3.01	38
cis-$[Pt(Me)_2(PR_3)_2]$	13	−6.0 ± 1	4.0 ± 0.4	−8.9 ± 1	24 ± 5	1338 ± 58	149	0.985	3.45	36
cis-$[Pt(Me)_2(PR_3)(Me_2SO)]$[d]	6	−7.2 ± 0.8				2001 ± 10		0.958	2.49	39
cis-$[Pt(Me)_2(PR_3)(py)]$[d]	6	−8.1 ± 0.9				2053 ± 10		0.949	2.31	39
cis-$[PtCl_2(PR_3)_2]$[d]	6	−8.9 ± 0.3				3796 ± 4		0.995	4.60	37
cis-$[PtMeCl(PR_3)_2]$[d]	5[e]	−3.4 ± 0.3				4543 ± 4		0.981	3.16	37
	5[f]	−10.5 ± 0.7				1868 ± 10		0.986	3.45	

[a] Number of data points. [b] Coefficient of determination. [c] Model selection criterion. [d] Regression analysis relative to isosteric phosphanes only. [e] $^1J_{PtP}$ for PR_3 trans to chloride. [f] $^1J_{PtP}$ for PR_3 trans to methyl group.

chloride, −10.5 ± 0.7 with PR_3 trans to the methyl group. Setting apart a comparison among the trans complexes, which is complicated by the fact that the ligand trans to PR_3 is another PR_3 that is different in each complex, it would seem that for uncharged species, the more electron withdrawing the substituent the smaller the $^1J_{PtP}$, while for cationic species the effect is opposite. This latter behavior corresponds to that of electron-rich platinum(0) complexes that has been rationalized on the basis of π-bonding effects.[37] Electron withdrawing should favor the metal-to-phosphorus π acceptance and involve a synergistic increase of the phosphorus-to-metal σ donation, which strengthens the bond and is accompanied by an increase in $^1J_{PtP}$.[37] This explanation clearly does not apply to cationic platinum(II) species, and in addition, an essential tenet of the QALE analysis is that π effects are absent in alkyl- and arylphosphanes $P(4\text{-}XC_6H_4)_3$ used as P-donor ligands.

A rationale for the pattern of behavior exhibited by the dependencies of the NMR data is not straightforward since the direction and the extent of stereoelectronic effects on the value of $^1J_{PtP}$ coupling constants appear to depend on the nature of groups attached to phosphorus,[40] the trans activating group,[34] the chelate ring size,[41] the platinum oxidation state,[42] the platinum−phosphorus bond length,[43] and as seen above, by the geometry and charge of the complex. Perhaps we would limit the interpretation of the $^1J_{PtP}$ electronic profiles to the simple observation of whether electron donation from substituents increases the covalent character and the strength of the Pt−P bond.

Steric effects also play a significant role.[36,44] Above the steric threshold, the overload of steric congestion leads to a sharp decrease of $^1J_{PtP}$ that must be associated with severe distortions of the bond angles and lengthening of Pt−P bond distances.[45] Under these circumstances, steric repulsion prevents maximum overlap of phosphorus- and platinum-bonding orbitals and changes the s character present in the metal−phosphorus bond. Thus, the steric threshold in the plot of $^1J_{PtP}$ vs the cone angles (Figure 10B), and the sharp change in the direction of the steric effects at 150°, can be assumed as a signal that marks the onset of significant changes in the structure of the $[Pt(Me)(Me_2\text{-phen})(PR_3)]^+$ complexes. This behavior is analogous to that found for *cis*-$[Pt(PR_3)_2Me_2]$ complexes[36] and has been confirmed recently by Nolan et al.[46] by determining the reaction enthalpies of a variety of such complexes and the X-ray molecular structures when PR_3 = PEt_3, PMe_2Ph, $P(pyrrolyl)_3$, and PCy_3. The relative stability of the dimethyl-bisphosphane platinum(II) complexes was found to be strongly influenced by the size of the phosphane, with larger cone angles resulting in less thermodynamically stable complexes. For instance, *cis*-$[Pt(PCy_3)_2Me_2]$ (PCy_3, θ =170°) has the lowest value of enthalpy of formation ($-\Delta H$ = 19.2 kcal/mol), the longer Pt−P bond separation (2.344(1) Å), and the largest P−Pt−P bond angle (P_1-Pt-P_2 = 108.60(5)°).

Potential Energy Surface and Flipping Mechanism. The stereoelectronic analysis of the coupling constants $^1J_{PtP}$ for **1**−**14** has shown that there is an efficient flow of charge density along the P−Pt−N axis on changing the basicity (χ values) of the coordinated phosphane. This electron flow also affects the individual rates of the various complexes, as shown by the linear correlation of the free energy of activation $\Delta G^{\ddagger}$ with χ in Figure 9A. However, the steric plot in Figure 9B, which describes the steric dependence of the free activation energies of these reactions and the sensitivity of the Me_2-phen flipping to steric effects, is particularly diagnostic in assessing the flipping mechanism. The shape of the steric plot is that expected for a purely dissociative process[47] and has been found in a number of dissociative substitutions on carbonyl compounds.[48] The steric dependence is the result of the different response of the energy of

(40) Pregosin, P. S.; Kunz, R. W. In *^{31}P and ^{13}C NMR of Transition Metal Complexes*; Diehl, P., Fluck, E., Kosfeld, R., Eds.; Springer: New York, 1979.
(41) Garrou, P. E. *Inorg. Chem.* **1975**, *14*, 1435−1439.
(42) Pregosin, P. S. Phosphorus-31 NMR Spectroscopy in Stereochemical Analysis. In *Organic Compounds and Metal Complexes*; Verkade, J. G., Quin, L. D., Eds.; VCH: New York, 1987; Chapter13 and references therein.
(43) (a) Mather, G. G.; Pidcock, A.; Rapsey, G. J. N. *J. Chem. Soc., Dalton Trans.* **1973**, 2095−2099. (b) Crispini, A.; Harrison, K. N.; Orpen, A. G.; Pringle, P. G.; Wheatcroft, J. R. *J. Chem. Soc., Dalton Trans.* **1996**, 1069−1076.
(44) Romeo, R. *Comments Inorg. Chem.* **2002**, *23*, 79−100.
(45) (a) Clark, H. C.; Hampden-Smith, M. J. *Coord. Chem. Rev.* **1987**, *79*, 229−255 and references therein. (b) Immirzi, A.; Musco, A.; Mann, B. E. *Inorg. Chim. Acta* **1977**, *21*, L37−L38. (c) Clark, H. C.; Nicholas, A.; Martin de P. *Magn. Reson. Chem.* **1990**, *28*, 99−103.
(46) Haar, C. M.; Nolan, P. S.; Marshall, W. J.; Moloy, K. G.; Prock, A.; Giering, W. P. *Organometallics* **1999**, *18*, 474−479.
(47) Ericks, K.; Giering, W. P.; Liu, H. Y.; Prock, A. *Inorg. Chem.* **1989**, *28*, 1759−1763.

Chart 2

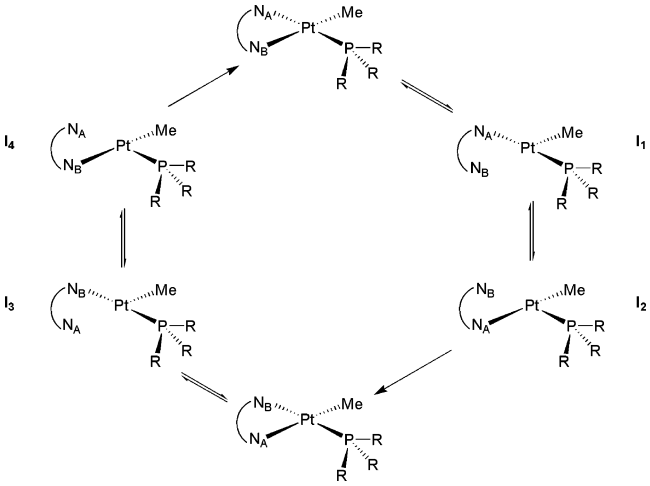

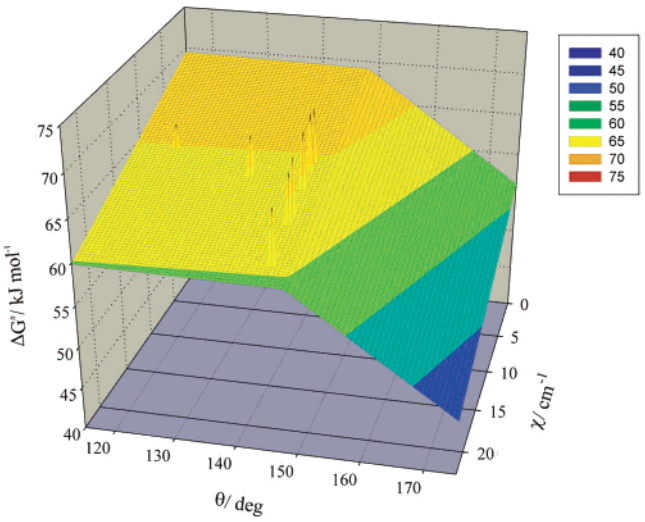

Figure 11. Free energy surface calculated for all possible combinations of χ and θ. The spikes account for the contribution from E_{ar}.

the ground and the transition states to changes in the size of the "spectator" ligands. The first horizontal upper part, for the ligands that fall before the steric threshold ($\theta < \theta_{ster}$), limits a region where steric effects are not operative both in the ground and in the transition state. The value of the steric threshold ($\theta_{ster} = 148°$) is almost coincident with that derived from the $^1J_{PtP}$ analysis ($\theta_{ster} = 150°$) and, as in the latter, marks the onset of steric destabilization of the ground state. In contrast, in bimolecular associative processes, when steric effects come into play, they are operative through a continuous destabilization of the transition state.[35−38]

There is significant release of steric strain if one arm of the Me_2-phen ligand dissociates from the highly congested four-coordinate $[Pt(Me)(Me_2\text{-phen})(PR_3)]^+$ compounds to a more flexible three-coordinate T-shaped intermediate. A dissociative mechanism, such as that illustrated in Chart 2, involves (i) platinum−nitrogen bond breaking and the formation of the two T-shaped intermediates I_1 and I_3, (ii) their isomerization into the corresponding intermediates I_2 and I_4, and (iii) finally, ring closing. In any event there is another flip possible, one which keeps the N atoms attached in the same location but interconverts enantiomers. This apparently occurs at lower temperatures since the potentially diastereotopic methyls in phosphane **8** are equivalent. Hence, there is presumably Pt−N bond breaking occurring rapidly at low temperature, but the "flipping" observed at the higher temperature is really associated with the T-shaped intermediate, allowing the monohapto complex to shift the single bond from trans to P to trans to Me (I_1 to I_2). The mechanism has already been proposed for the fluxional motion of Me_2-phen when $PR_3 = P(C_6H_5)_3$,[1] and applies to all the series of related compounds in view of the absence of potential reagents and considering that the solvent or the BArf counterion is too weakly coordinating to promote a nucleophilic attack and reaction pathways via five-coordinate species. An alternative intramolecular twist rotation pathway is accessible only to photochemical activation[49] or in a rare case in which the molecule already has a strong tetrahedral distortion in the ground state, as reported recently for the fluxional behavior of *cis*-bis(silyl)bis(phosphane)platinum(II).[50] The process features an uncatalyzed isomerization, many examples of which can be found in the literature.[36] The interconversion of two η^1-coordinate three-coordinate species is also demonstrated for the dynamic behavior of bidentate nitrogen ligands in some palladium(II) complexes.[51]

A free-energy surface representing the general σ basicity and steric effects in a dissociative process is shown in Figure 11 and has been constructed using the results from regression analysis (eq 2), according to a method recently proposed by Poë et al.[15d,52] for associative reactions of metal−carbonyl clusters. This type of plot predicts the way in which a P-donor ligand should affect the energy of the transition state in the absence of aryl or π-acidity effects. The spikes indicate the additional contribution due to the aryl effect for some phosphorus ligands.

Conclusions

The severe distortion of the bidentate nitrogen ligand 2,9-dimethyl-1,10-phenanthroline in alkyl platinum(II) complexes of the type $[Pt(Me)(Me_2\text{-phen})(PR_3)]^+$ and the lengthening of the Pt−N bonds are at the origin of its fluxional motion between different exchanging sites. The $^1J_{PtP}$ coupling

(48) (a) Babij, C.; Chen, L.; Koshevoy, I. O.; Poë, A. J. *J. Chem Soc., Dalton Trans.* **2004**, 833−838. (b) Chalk, K. L.; Pomeroy, R. K. *Inorg. Chem.* **1984**, *23*, 444−449. (c) Chen, L.; Poë, A. J. *Inorg. Chem.* **1989**, *28*, 3641−3647. (d) Brodie, N. M. J.; Poë, A. J. *Can. J. Chem.* **1995**, *73*, 1187−1195.

(49) (a) Whitesides, T. H. *J. Am. Chem. Soc.* **1969**, *91*, 2395−2396. (b) Costanzo, L. L.; Giuffrida, S.; Romeo, R. *Inorg. Chim. Acta* **1980**, *38*, 31−35. (c) Price, J. H.; Birk, J. P.; Wayland, B. B. *Inorg. Chem.* **1978**, *17*, 2245−2250.

(50) (a) Tsuji, Y.; Nishiyama, K.; Hori, S.-Y.; Ebihara, M.; Kawamura, T. *Organometallics* **1998**, *17*, 507−512. (b) Obora, Y.; Tsuji, Y.; Nishiyama, K.; Ebihara, M.; Kawamura, T. *J. Am. Chem. Soc.* **1996**, *118*, 10922−10923.

(51) (a) Albinati, A.; Kunz, R. W.; Ammann, C. J.; Pregosin, P. S. *Organometallics* **1991**, *10*, 1800−1806. (b) Gogoll, A.; Ornebro, J.; Grennberg, H.; Bakwall, J. E. *J. Am. Chem. Soc.* **1994**, *116*, 3631−3632. (c) Delis, J. G. P.; Aubel, P. G.; Vrieze, K.; van Leeuwen, P. W. N. M.; Veldman, N.; Spek, A. L.; van Neer, F. J. R. *Organometallics* **1997**, *16*, 2948−2957.

(52) Bunte, K. A.; Farra, D. H.; Poë, A. J. *Organometallics* **2003**, *22*, 3448−3454.

constants of the complexes and the free activation energies for the flipping have been analyzed quantitatively, according to steric and electronic properties of the P-donor ligands by the QALE method. The results of the analysis on NMR and kinetic data are corroborated by the results of the structural studies, indicating that phosphorus ligands with cone angles greater than 150° cause an overload of steric congestion in the ground state. This remarkable steric congestion at the coordination plane favors the facile dissociation of the Pt−N bonds and the formation of a T-shaped η^1-ring-opened three-coordinate species whose fluxionality accounts for the dynamic behavior of the bidentate nitrogen ligand. The free-energy surface constructed with the results of the QALE analysis on the kinetic data gives a simple widespread graphical representation of the σ basicity and steric effects upon which the aryl effects are separately superimposed as additional peaks.

Experimental Section

General Procedures and Chemicals. All syntheses were performed under a dry, oxygen-free nitrogen atmosphere using standard Schlenk-tube techniques or in a glovebox containing less than 1 ppm of oxygen and water; however, the products may be worked up and handled in air. All solvents were analytical reagent grade (Lab-Scan Ltd) and were used in the synthetic procedures after distillation under a nitrogen atmosphere from appropriate drying agents: diethyl ether from sodium benzophenone ketyl, dichloromethane from barium oxide, dimethylsulfoxide, at low pressure, from CaH_2, after preliminary filtration through an alumina column. All solvents were stored in N_2-filled flasks over activated 4-Å molecular sieves. Chloroform-*d* (99.96+%, C. I. L. Inc.) was dried standing for many days over CaH_2, distilled under nitrogen over activated magnesium sulfate and sodium carbonate, and then stored over activated 4-Å molecular sieves. K_2PtCl_4 (Strem) was purified by dissolving it in water and filtering. The salt Na[B(3,5-$(CF_3)_2C_6H_3)_4$] was prepared according to the literature method.[53] All phosphane ligands used in these studies were purchased from Strem or Aldrich. Solid phosphanes were recrystallyzed from EtOH by dissolving in the hot solvent, filtering, and cooling the filtrate to 0 °C. The crystals were stored and used under nitrogen. All the other chemicals were the highest grade commercially available and were used as received.

Instrumentation. NMR spectra were recorded on a Bruker AMX R-300 spectrometer equipped with a broad-band probe operating at 300.13 and 121.50 MHz for ^{1}H and ^{31}P nuclei, respectively. Proton chemical shifts are reported in parts per million (δ/ppm) relative to tetramethylsilane (Me_4Si) as an internal standard (0.0 ppm) or referenced with the proton resonance resulting from incomplete deuteration of the NMR solvent ($CDCl_3$: 7.26 ppm). ^{31}P{^{1}H} NMR signals are reported in ppm (δ) relative to external 85% H_3PO_4 at 0.0 ppm. Coupling constants are given in hertz (*J*/Hz). Phase-sensitive ^{1}H 2D-NOESY experiments were performed with a standard pulse sequence by using a mixing time of 0.6 s. NMR samples were prepared by dissolving ~20 mg of compound in 0.5 mL of $CDCl_3$. The temperature within the probe was measured using the methanol or ethylene glycol method.[54] Elemental analyses were performed by Microanalytical Laboratory, Department of Chemistry, University College Dublin, Ireland.

Synthesis of Complexes. The complex *trans*-[Pt(Cl)(Me)(Me_2-$SO)_2$] was prepared according to Eaborn et al.[55] and was purified by several crystallizations from dichloromethane/diethyl ether mixtures. The complexes [Pt(Me)(Me_2-phen)(Me_2SO)]PF_6 and [Pt-(Me)(Me_2-phen)($P(C_6H_5)_3$)]PF_6 were prepared following published procedures.[1] The complexes [Pt(Me)(Me_2-phen)(P)]BArf (P = $P(C_6H_5)_3$ **1**, $P(4\text{-}FC_6H_4)_3$ **2**, $P(4\text{-}ClC_6H_4)_3$ **3**, $P(4\text{-}CF_3C_6H_4)_3$ **4**, $P(4\text{-}MeOC_6H_4)_3$ **5**, $P(4\text{-}MeC_6H_4)_3$ **6**, $PMe(C_6H_5)_2$ **7**, $PMe_2(C_6H_5)$ **8**, PMe_3 **9**, PEt_3 **10**, P(*i*-Pr)$_3$ **11**, $PCy(C_6H_5)_2$ **12**, $PCy_2(C_6H_5)$ **13**, and PCy_3 **14**) were prepared by using essentially the method described below for compound **3**.

[Pt(Me)(Me_2-phen)($P(4\text{-}ClC_6H_4)_3$)]BArf, 3. A dichloromethane solution (20 mL) of $P(4\text{-}ClC_6H_4)_3$ (118.4 mg, 0.324 mmol) was added dropwise under continuous stirring to a solution (20 mL) of [Pt(Me)(Me_2-phen)(Me_2SO)]PF_6 (207.8 mg, 0.324 mmol). Evaporation of most of the solvent, addition of diethyl ether, and cooling to −30 °C led to the separation of a powdery solid of [Pt(Me)-(Me_2-phen)($P(4\text{-}ClC_6H_4)_3$)]PF_6 **3a** (87.5% yield). This latter was dissolved again in dichloromethane, and the stoichiometric amount of Na[B(3,5-$(CF_3)_2C_6H_3)_4$] (251.6 mg, 0.284 mmol) was added. The white solid ($NaPF_6$) formed under stirring was filtered off, and evaporation of the solvent led to the formation of **3** (91% yield) as a brown solid.

[Pt(Me)(Me_2-phen)($P(C_6H_5)_3$)]BArf, 1: ^{1}H NMR ($CDCl_3$, T = 260 K): δ 8.32 (d, $^3J_{HH}$ = 8.3 Hz, 1H, H_4), 8.15 (d, $^3J_{HH}$ = 8.4 Hz, 1H, H_7), 7.75 (AB system, $^3J_{HH}$ = 8.9 Hz, 1H, H_5), 7.73 (AB system, $^3J_{HH}$ = 8.9 Hz, 1H, H_6), 7.73 (m, 8H, $H_{o,o'}$-BArf), 7.68 (d, $^3J_{HH}$ = 8.5 Hz, $^5J_{PH}$ = 1.3 Hz, 1H, H_3), 7.52 (d, $^3J_{HH}$ = 8.3 Hz, $^3J_{PH}$ = 10.5 Hz, 6H, $H_{o,o'}$-P), 7.52 (buried under $H_{o,o'}$-P, 3H, H_p-P), 7.48 (m, br, 4H, H_p-BArf), 7.38 (dd, $^3J_{HH}$ = 8.3 Hz, $^3J_{HH}$ = 6.9 Hz, $^4J_{PH}$ = 2.4 Hz, 6H, $H_{m,m'}$-P), 7.09 (d, $^3J_{HH}$ = 8.4 Hz, 1H, H_8), 3.02 (s, 3H, Me_A), 1.90 (s, 3H, Me_B), 0.74 (s, $^2J_{PtH}$ = 66.9 Hz, $^3J_{PH}$ = 4.1 Hz, 3H, Pt-CH_3). ^{31}P{^{1}H} NMR ($CDCl_3$): δ 14.3 (s, $^1J_{PtP}$ = 4575 Hz). Anal. Calcd for $C_{65}H_{42}BF_{24}N_2PPt$: C, 50.57; H, 2.74; N, 1.81. Found: C, 50.71; H, 2.83; N, 1.85.

[Pt(Me)(Me_2-phen)($P(4\text{-}FC_6H_4)_3$)]BArf, 2: ^{1}H NMR ($CDCl_3$, T = 260 K): δ 8.32 (d, $^3J_{HH}$ = 8.4 Hz, 1H, H_4), 8.21 (d, $^3J_{HH}$ = 8.4 Hz, 1H, H_7), 7.76 (s, 2H, $H_{5,6}$), 7.72 (m, br, 8H, $H_{o,o'}$-BArf), 7.67 (d, $^3J_{HH}$ = 8.4 Hz, 1H, H_3), 7.51 (m, 6H, $H_{o,o'}$-P), 7.46 (m, br, 4H, H_p-BArf), 7.16 (d, $^3J_{HH}$ = 8.4 Hz, 1H, H_8), 7.09 (m, 6H, $H_{m,m'}$-P), 2.99 (s, 3H, Me_A), 1.92 (s, 3H, Me_B), 0.69 (s, $^2J_{PtH}$ = 74.0 Hz, $^3J_{PH}$ = 4.4 Hz, 3H, Pt-CH_3). ^{31}P NMR ($CDCl_3$): δ 12.3 ($^1J_{PtP}$ = 4618 Hz). Anal. Calcd for $C_{65}H_{39}BF_{27}N_2PPt$: C, 48.86; H, 2.46; N, 1.75. Found: C, 48.46; H, 2.95; N, 1.36.

[Pt(Me)(Me_2-phen)($P(4\text{-}ClC_6H_4)_3$)]BArf, 3: ^{1}H NMR ($CDCl_3$, T = 260 K): δ 8.33 (d, $^3J_{HH}$ = 8.4 Hz, 1H, H_4), 8.26 (d, $^3J_{HH}$ = 8.4 Hz, 1H, H_7), 7.78 (s, 2H, $H_{5,6}$), 7.73 (m, br, 8H, $H_{o,o'}$-BArf), 7.68 (d, $^3J_{HH}$ = 8.4 Hz, 1H, H_3), 7.47 (m, br, 4H, H_p-BArf), 7.40 (m, br, 12H, $H_{o,o'}$-P + $H_{m,m'}$-P), 7.20 (d, $^3J_{HH}$ = 8.4 Hz, 1H, H_8), 3.00 (s, 3H, Me_A), 1.95 (s, 3H, Me_B), 0.69 (s, $^2J_{PtH}$ = 74.4 Hz, $^3J_{PH}$ = 4.4, 3H, Pt-CH_3). ^{31}P NMR ($CDCl_3$): δ 13.2 ($^1J_{PtP}$ = 4622 Hz). Anal. Calcd for $C_{65}H_{39}BCl_3F_{24}N_2PPt$: C, 47.40 H, 2.39; N, 1.70. Found: C, 47.84; H, 2.75; N, 1.64.

[Pt(Me)(Me_2-phen)($P(4\text{-}CF_3C_6H_4)_3$)]BArf, 4: ^{1}H NMR ($CDCl_3$, T = 260 K): δ 8.27 (d, $^3J_{HH}$ = 8.4 Hz, 1H, H_4), 8.18 (d, $^3J_{HH}$ = 8.4 Hz, 1H, H_7), 7.69 (m, br, 21H, H_3 + $H_{o,o'}$-BArf + $H_{o,o'}$-P + $H_{m,m'}$-P), 7.63 (s, 2H, $H_{5,6}$), 7.43 (m, br, 4H, H_p-BArf), 7.08 (d, $^3J_{HH}$ = 8.4 Hz, 1H, H_8), 2.97 (s, 3H, Me_A), 1.86 (s, 3H, Me_B), 0.73 (s, $^2J_{PtH}$ = 70.0 Hz, $^3J_{PH}$ = 4.4 Hz, 3H, Pt-CH_3). ^{31}P NMR

(53) Brookhart, M.; Grant, B.; Volpe, A. F. *Organometallics* **1992**, *11*, 3920−3922.
(54) (a) Van Geet, A. L. *Anal. Chem.* **1968**, *40*, 2227−2229. (b) Van Geet, A. L. *Anal. Chem.* **1970**, *42*, 679−680.
(55) Eaborn, C.; Kundu, K.; Pidcock, A. *J. Chem. Soc., Dalton Trans.* **1981**, 933−938.

($CDCl_3$): δ 15.1 ($^1J_{PtP}$ = 4656 Hz). Anal. Calcd for $C_{68}H_{39}BF_{33}N_2$PPt: C, 46.73; H, 2.25; N, 1.60. Found: C, 46.22; H, 2.21; N, 1.56.

[Pt(Me)(Me$_2$-phen)(P(4-MeOC$_6$H$_4$)$_3$)]BArf, 5: ^{1}H NMR ($CDCl_3$, T = 260 K): δ 8.32 (d, $^3J_{HH}$ = 8.4 Hz, 1H, H_4), 8.18 (d, $^3J_{HH}$ = 8.4 Hz, 1H, H_7), 7.76 (s, 2H, $H_{5,6}$), 7.73 (m, br, 8H, $H_{o,o'}$-BArf), 7.67 (d, $^3J_{HH}$ = 8.4 Hz, 1H, H_3), 7.49 (m, br, 4H, H_p-BArf), 7.46 (m, 6H, $H_{o,o'}$-P), 7.16 (d, $^3J_{HH}$ = 8.4 Hz, 1H, H_8), 6.87 (m, 6H, $H_{m,m'}$-P), 3.81 (s, 9H, O-CH_3), 3.02 (s, 3H, Me_A), 2.02 (s, 3H, Me_B), 0.75 (s, $^2J_{PtH}$ = 75.2 Hz, $^3J_{PH}$ = 4.4 Hz, 3H, Pt-CH_3). ^{31}P NMR ($CDCl_3$): δ 9.8 ($^1J_{PtP}$ = 4561 Hz). Anal. Calcd for $C_{68}H_{48}BF_{24}N_2O_3$PPt: C, 49.99; H, 2.96; N, 1.71. Found: C, 49.65; H, 3.14; N, 1.70.

[Pt(Me)(Me$_2$-phen)(P(4-MeC$_6$H$_4$)$_3$)]BArf, 6: ^{1}H NMR ($CDCl_3$, T = 298 K): δ 8.33 (d, $^3J_{HH}$ = 8.3 Hz, 1H, H_4), 8.15 (d, $^3J_{HH}$ = 8.3 Hz, 1H, H_7), 7.77 (AB system, $^3J_{HH}$ = 9.3 Hz, 1H, H_5), 7.75 (AB system, $^3J_{HH}$ = 9.3 Hz, 1H, H_6), 7.70 (m, br, 8H, $H_{o,o'}$-BArf), 7.67 (d, $^3J_{HH}$ = 8.3 Hz, 1H, H_3), 7.47 (m, br, 4H, H_p-BArf), 7.41 (d, $^3J_{HH}$ = 8.1 Hz, $^3J_{PH}$ = 11.4 Hz, 6H, $H_{o,o'}$-P), 7.15 (d, $^3J_{HH}$ = 8.1 Hz, $^3J_{PH}$ = 1.9 Hz, 6H, $H_{m,m'}$-P), 7.09 (d, $^3J_{HH}$ = 8.3 Hz, 1H, H_8), 3.02 (s, 3H, Me_A), 2.37 (s, 9H, P-CH_3), 1.95 (s, 3H, Me_B), 0.73 (s, $^2J_{PtH}$ = 74.5 Hz, $^3J_{PH}$ = 4.2 Hz, 3H, Pt-CH_3). ^{31}P NMR ($CDCl_3$): δ 12.0 ($^1J_{PtP}$ = 4557 Hz). Anal. Calcd for $C_{68}H_{48}BF_{24}N_2$PPt: C, 51.50; H, 3.05; N, 1.77. Found: C, 51.65; H, 3.12; N, 1.70.

[Pt(Me)(Me$_2$-phen)(PMe(C$_6$H$_5$)$_2$)]BArf, 7: ^{1}H NMR ($CDCl_3$, T = 240 K): δ 8.30 (d, $^3J_{HH}$ = 8.3 Hz, 1H, H_4), 8.10 (d, $^3J_{HH}$ = 8.3 Hz, 1H, H_7), 7.72 (m, br, 10H, $H_{5,6}$ + $H_{o,o'}$-BArf), 7.64 (d, $^3J_{HH}$ = 8.3 Hz, 1H, H_3), 7.46 (m, br, 8H, H_p-BArf + $H_{o,o'}$-P), 7.37 (m, 6H, $H_{m,m'}$-P + H_p-P), 7.03 (d, $^3J_{HH}$ = 8.3 Hz, 1H, H_8), 3.02 (s, 3H, Me_A), 1.97 (s, 3H, Me_B), 1.94 (s, $^3J_{PtH}$ = 52.7 Hz, $^2J_{PH}$ = 10.1 Hz, 3H, P-CH_3), 0.90 (s, $^2J_{PtH}$ = 72.5 Hz, $^3J_{PH}$ = 3.9 Hz, 3H, Pt-CH_3). ^{31}P NMR ($CDCl_3$): δ −1.0 ($^1J_{PtP}$ = 4534 Hz). Anal. Calcd for $C_{60}H_{40}BF_{24}N_2$PPt: C, 48.63; H, 2.72, N, 1.89. Found: C, 48.75; H, 2.80; N, 1.82.

[Pt(Me)(Me$_2$-phen)(PMe$_2$(C$_6$H$_5$))]BArf, 8: ^{1}H NMR ($CDCl_3$, T = 240 K): δ 8.31 (d, $^3J_{HH}$ = 8.3 Hz, 1H, H_4), 8.13 (d, $^3J_{HH}$ = 8.3 Hz, 1H, H_7), 7.83 (s, 2H, $H_{5,6}$), 7.70 (m, br, 8H, $H_{o,o'}$-BArf), 7.66 (d, $^3J_{HH}$ = 8.3 Hz, 1H, H_3), 7.45 (s, br, 4H, H_p-BArf), 7.42−7.22 (m, br, 5H, $H_{o,o'}$-P + $H_{m,m'}$-P + H_p-P), 7.09 (d, $^3J_{HH}$ = 8.3 Hz, 1H, H_8), 3.02 (s, 3H, Me_A), 2.13 (s, 3H, Me_B), 1.76 (s, $^3J_{PtH}$ = 47.4 Hz, $^2J_{PH}$ = 10.1 Hz, 6H, P-CH_3), 1.00 (s, $^2J_{PtH}$ = 74.2 Hz, $^3J_{PH}$ = 4.4 Hz, 3H, Pt-CH_3). ^{31}P NMR ($CDCl_3$): δ −18.1 ($^1J_{PtP}$ = 4379 Hz). Anal. Calcd for $C_{55}H_{38}BF_{24}N_2$PPt: C, 46.53; H, 2.70; N, 1.97. Found: C, 46.80; H, 2.73; N, 2.00.

[Pt(Me)(Me$_2$-phen)(P(Me)$_3$)]BArf, 9: ^{1}H NMR ($CDCl_3$, T = 270 K): δ 8.31 (d, $^3J_{HH}$ = 8.3 Hz, 1H, H_4), 8.25 (d, $^3J_{HH}$ = 8.3 Hz, 1H, H_7), 7.75 (AB system, $^3J_{HH}$ = 9.2 Hz, 1H, H_5), 7.72 (AB system, $^3J_{HH}$ = 9.2 Hz, 1H, H_6), 7.70 (m, br, 8H, $H_{o,o'}$-BArf), 7.64 (d, $^3J_{HH}$ = 8.3 Hz, 1H, H_3), 7.57 (d, $^3J_{HH}$ = 8.3 Hz, 1H, H_8), 7.47 (m, br, 4H, H_p-BArf), 2.97 (s, 3H, Me_A), 2.91 (s, 3H, Me_B), 1.46 (s, $^3J_{PtH}$ = 45.2 Hz, $^2J_{PH}$ = 10.5 Hz, 9H, P-CH_3), 0.92 (s, $^2J_{PtH}$ = 72.9 Hz, $^3J_{PH}$ = 4.39 Hz, 3H, Pt-CH_3). ^{31}P {^{1}H} NMR ($CDCl_3$): δ −31.8 ($^1J_{PtP}$ = 4291 Hz). Anal. Calcd for $C_{50}H_{36}BF_{24}N_2$PPt: C, 44.23; H, 2.67; N, 2.06. Found: C, 43.97; H, 2.37; N, 1.99.

[Pt(Me)(Me$_2$-phen)(P(Et)$_3$)]BArf, 10: ^{1}H NMR ($CDCl_3$, T = 220 K): δ 8.25 (d, $^3J_{HH}$ = 8.3 Hz, 1H, H_4), 8.18 (d, $^3J_{HH}$ = 8.3 Hz, 1H, H_7), 7.74 (m, br, 8H, $H_{o,o'}$-BArf), 7.69 (AB system, $^3J_{HH}$ = 9.7 Hz, 1H, H_5), 7.67 (AB system, $^3J_{HH}$ = 9.7 Hz, 1H, H_6), 7.61 (d, $^3J_{HH}$ = 8.3 Hz, 1H, H_3), 7.53 (d, $^3J_{HH}$ = 8.3 Hz, 1H, H_8), 7.47 (m, br, 4H, H_p-BArf), 2.95 (s, 3H, Me_A), 2.91 (s, 3H, Me_B), 1.72 (m, 6H, P-CH_2CH$_3$), 0.87 (m, 9H, P-CH$_2$CH_3), 0.84 (s, $^2J_{PtH}$ = 72.5 Hz, $^3J_{PH}$ = 3.0 Hz, 3H, Pt-CH_3). ^{31}P NMR ($CDCl_3$): δ 3.4 ($^1J_{PtP}$ = 4327 Hz). Anal. Calcd for $C_{53}H_{42}BF_{24}N_2$PPt: C, 45.48; H, 3.02; N, 2.00. Found: C, 44.98 H, 2.93; N, 1.98.

[Pt(Me)(Me$_2$-phen)(P(*i*-Pr)$_3$)]BArf, 11: ^{1}H NMR ($CDCl_3$, T = 255 K): δ, 8.23 (d, $^3J_{HH}$ = 8.3 Hz, 1H, H_4), 8.22 (d, $^3J_{HH}$ = 8.3 Hz, 1H, H_7), 7.72 (m, br, 10H, $H_{5,6}$ + $H_{o,o'}$-BArf), 7.58 (d, $^3J_{HH}$ = 8.3 Hz, 1H, H_3), 7.54 (d, $^3J_{HH}$ = 8.3 Hz, 1H, H_8), 7.48 (m, br, 4H, H_p-BArf), 2.94 (s, 3H, Me_A), 2.92 (s, 3H, Me_B), 2.32 (m, 3H, P-CHCH$_3$), 1.04 (m, 18H, P-CHCH_3), 0.96 (s, $^2J_{PtH}$ = 73.8 Hz, $^3J_{PH}$ = 2.2 Hz, 3H, Pt-CH_3). ^{31}P NMR ($CDCl_3$): δ 23.9 ($^1J_{PtP}$ = 4358 Hz). Anal. Calcd for $C_{56}H_{48}BF_{24}N_2$PPt: C, 46.65; H, 3.36; N, 1.94. Found: C, 46.58; H, 3.00; N, 1.92.

[Pt(Me)(Me$_2$-phen)(PCy(C$_6$H$_5$)$_2$)]BArf, 12: ^{1}H NMR ($CDCl_3$, T = 290 K): δ 8.29 (d, $^3J_{HH}$ = 8.3 Hz, 1H, H_4), 8.18 (d, $^3J_{HH}$ = 8.4 Hz, 1H, H_7), 7.72 (s, 2H, $H_{5,6}$), 7.73 (m, br, 8H, $H_{o,o'}$-BArf), 7.67 (d, $^3J_{HH}$ = 8.3 Hz, 1H, H_3), 7.49 (m, br, 4H, H_p-BArf), 7.40 (m, br, 10H, $H_{o,o'}$-P + $H_{m,m'}$-P + H_p-P), 7.15 (d, $^3J_{HH}$ = 8.4 Hz, 1H, H_8), 2.98 (s, 3H, Me_A), 2.62 (m, 1H, P-CH), 2.01 (s, 3H, Me_B), 1.91 (m, 2H, C-CH_2), 1.62 (m, 3H, C-CH_2), 1.25 (m, 2H, C-CH_2), 0.95 (s, $^2J_{PtH}$ = 70.3 Hz, $^3J_{PH}$ = 3.1 Hz, 3H, Pt-CH_3), 0.88 (m, 3H, C-CH_2). ^{31}P NMR ($CDCl_3$): δ 13.7 ($^1J_{PtP}$ = 4501 Hz). Anal. Calcd for $C_{65}H_{48}BF_{24}N_2$PPt: C, 50.37; H, 3.12; N, 1.81. Found: C, 50.22; H, 3.06; N, 1.78.

[Pt(Me)(Me$_2$-phen)(PCy$_2$(C$_6$H$_5$))]BArf, 13: ^{1}H NMR ($CDCl_3$, T = 298 K): δ 8.33 (d, $^3J_{HH}$ = 8.3 Hz, 1H, H_4), 8.22 (d, $^3J_{HH}$ = 8.3 Hz, 1H, H_7), 7.79 (s, 2H, $H_{5,6}$), 7.72 (m, br, 8H, $H_{o,o'}$-BArf), 7.68 (d, $^3J_{HH}$ = 8.3 Hz, 1H, H_3), 7.49 (m, br, 4H, H_p-BArf), 7.44 (dd, $^3J_{HH}$ = 7.7 Hz, $^4J_{HH}$ = 1.3 Hz, 1H, H_p-P), 7.20 (d, $^3J_{HH}$ = 7.9 Hz, $^3J_{PH}$ = 9.4 Hz, 2H, $H_{o,o'}$-P), 7.14 (d, $^3J_{HH}$ = 8.3 Hz, 1H, H_8), 6.93 (dd, $^3J_{av}$ = 7.8 Hz, 2H, $H_{m,m'}$-P), 3.03 (s, 3H, Me_A), 2.48 (m, 2H, P-CH), 1.98−1.54 (m, 10H, C-CH_2), 1.85 (s, 3H, Me_B), 1.47−1.05 (m, 10H, C-CH_2), 1.03 (s, $^2J_{PtH}$ = 72.9 Hz, $^3J_{PH}$ = 3.1 Hz, 3H, Pt-CH_3). ^{31}P NMR ($CDCl_3$): δ 11.8 ($^1J_{PtP}$ = 4287 Hz). Anal. Calcd for $C_{65}H_{54}BF_{24}N_2$PPt: C, 50.17; H, 3.50; N, 1.80. Found: C, 50.30; H, 3.65; N, 1.82.

[Pt(Me)(Me$_2$-phen)(P(Cy)$_3$]BArf, 14: ^{1}H NMR ($CDCl_3$, T = 255 K): δ 8.29 (d, $^3J_{HH}$ = 8.3 Hz, 1H, H_4), 8.25 (d, $^3J_{HH}$ = 8.3 Hz, 1H, H_7), 7.72 (m, br, 10H, $H_{5,6}$ + $H_{o,o'}$-BArf), 7.64 (d, $^3J_{HH}$ = 8.3 Hz, 1H, H_3), 7.59 (d, $^3J_{HH}$ = 8.3 Hz, 1H, H_8), 7.48 (m, br, 4H, H_p-BArf), 3.00 (s, 3H, Me_A), 2.93 (s, 3H, Me_B), 2.09 (m, br, 3H, P-CH), 1.68 (m, br, 12H, C-CH_2), 1.42 (m, br, 6H, C-CH_2), 1.14 (m, br, 12H, C-CH_2), 0.93 (s, $^2J_{PtH}$ = 74.6 Hz, 3H, Pt-CH_3). ^{31}P NMR ($CDCl_3$): δ 13.0 ($^1J_{PtP}$ = 4315 Hz). Anal. Calcd for $C_{65}H_{60}BF_{24}N_2$PPt: C, 49.98; H, 3.87; N, 1.79. Found: C, 49.85; H, 3.92; N, 1.82.

[Pt(Me)(phen)(P(C$_6$H$_5$)$_3$)]PF$_6$, 15. The complex [Pt(Me)(Cl)(phen)] (50 mg, 0.117 mmol) was dissolved in 20 mL of dichloromethane, and a dichloromethane solution of $AgPF_6$ (29.6 mg, 0.117 mmol) was added dropwise with continuous stirring. Upon precipitation of AgCl, the color of the solution slowly changed from yellow to colorless. After filtration of AgCl, the phosphane was added cautiously ($P(C_6H_5)_3$, 30.7 mg, 0.117 mmol in 10 mL of dichloromethane), the solution was filtered on cellulose powder to remove residual AgCl and concentrated by a rotavapor. *n*-Hexane was added, and the mixture was cooled to −35 °C to give 88 mg of **15** as an off-white solid (yield: 95%).

^{1}H NMR ($CDCl_3$, T = 298 K): δ 9.33 (dd, $^3J_{PtH}$ = 35.2 Hz, $^3J_{HH}$ = 5.5 Hz, $^4J_{HH}$ = 1.1 Hz, $^4J_{PH}$ = 3.8 Hz, 1H, H_2), 8.88 (dd, $^3J_{HH}$ = 8.2 Hz, $^4J_{HH}$ = 1.1 Hz, 1H, H_4), 8.68 (dd, $^3J_{HH}$ = 8.2 Hz, $^4J_{HH}$ = 1.1 Hz, 1H, H_7), 8.18 (dd, $^3J_{HH}$ = 5.5, 8.2 Hz, 1H, H_3), 8.14 (AB system, $^3J_{HH}$ = 8.8 Hz, 1H, H_5), 8.12 (AB system, $^3J_{HH}$ = 8.8 Hz, 1H, H_6), 7.80 (dd, $^3J_{PH}$ = 11.5 Hz, $^3J_{HH}$ = 8.2 Hz, $^4J_{HH}$ = 1.6 Hz, 6H, $H_{o,o'}$-P), 7.69 (dd, $^3J_{PtH}$ = 17.0 Hz, $^3J_{HH}$ = 5.5 Hz, $^4J_{HH}$ = 1.1 Hz, 1H, H_9), 7.59 (dd, $^3J_{HH}$ = 5.5, 8.2 Hz, 1H, H_8),

Table 5. Experimental Data for the X-ray Diffraction Study of Compounds: **8**, **11**, **14**, and **15**[a]

	8	**11**	**14**	**15**
formula	$C_{55}H_{38}BF_{24}N_2PPt$	$C_{56}H_{48}BF_{24}N_2PPt$	$C_{65}H_{57}BF_{24}N_2PPt$	$C_{31}H_{26}F_6N_2P_2Pt$
mol wt	1419.74	1441.83	1559.00	797.59
data coll *T*, K	293(2)	153(2)	293(2)	183(2)
cryst syst	triclinic	triclinic	orthorhombic	monoclinic
space group (no.)	$P\bar{1}$ (2)	$P\bar{1}$ (2)	*Aba*2 (41)	*P*21/*n* (14)
a, Å	12.785(1)	13.941(5)	39.568(2)	14.197(1)
b, Å	14.513(2)	14.030(5)	17.767(2)	30.075(2)
c, Å	16.986(2)	17.490(6)	19.237(4)	20.940(2)
α, deg	103.605(2)	102.594(8)	90	90
β, deg	105.925(3)	109.181(9)	90	107.275(2)
γ, deg	101.266(2)	108.253(8)	90	90
V, Å^3	2829.5(5)	2865(2)	13524(3)	8538(1)
Z	2	2	8	12
$\rho_{(calcd)}$, g cm^{-3}	1.666	1.671	1.531	1.861
μ, cm^{-1}	26.26	25.94	22.05	51.08
θ range, (deg)	$2.45 < \theta < 27.03$	$1.64 < \theta < 26.01$	$1.22 < \theta < 26.03$	$1.95 < \theta < 26.00$
no. data collected	25322	28013	60775	80178
no. independent data	12412	13272	16808	10915
no. obs reflns (n_o) $[\|F_o\|^2 > 2.0\sigma(\|F\|^2)]$	9862	8743	9591	13988
no. of params refined(n_v)	766	903	1135	869
abs structure (Flack's) param	0.023(8)	0.023(8)	0.023(8)	0.023(8)
R_{av}[b]	0.0283	0.0461	0.0701	0.0437
R (obs reflns)[b]	0.0275	0.067	0.0465	0.0277
wR2 (obs reflns)[b]	0.0722	0.1674	0.0805	0.0603
GOF[b]	0.930	0.996	0.994	1.039

[a] Diffractometer, Bruker SMART CCD; radiation, Mo Kα (graphite monochrom, $\lambda = 0.71073$ Å. [b] $R_{av} = \sum|F_o^2 - F_{o,\,av}^2|/\sum_i |F_o^2|$; $R = \sum(|F_o - (1/k)F_c|)/\sum|F_o|$; wR2 $= [\sum w(F_o^2 - (1/k)F_c^2)^2/\sum w\,|F_o^2|^2]^{1/2}$; GOF $= [\sum_w(F_o^2 - (1/k)F_c^2)^2/(n_o - n_v)]^{1/2}$.

7.56 (m, $^3J_{HH} = 7.7$ Hz, $^4J_{HH} = 1.6$ Hz, 3H, H_p-P), 7.49 (dd, $^3J_{HH} = 7.7$, 8.2 Hz, $^4J_{PH} = 2.2$ Hz, 6H, $H_{m,m'}$-P), 0.92 (s, $^2J_{PtH} = 69.8$ Hz, $^3J_{PH} = 3.3$ Hz, 3H, Pt-*CH*$_3$). $^{31}P\{^1H\}$ NMR ($CDCl_3$): δ 19.1 (s, $^1J_{PtP} = 4395$ Hz), −144.1 ($^1J_{FP} = 714$ Hz). Anal. Calcd for $C_{31}H_{26}F_6N_2P_2Pt$: C, 46.68; H, 3.29; N, 3.51. Found: C, 46.77; H, 3.17; N, 3.57.

Variable-Temperature NMR Experiments. In a typical experiment, approximately 20 mg of the complex was dissolved in the appropriate volume of deuterated solvent (∼0.5 mL). The ^1H NMR spectrum was recorded over a temperature range depending on the rate of the fluxional motion (from 219 to 354 K for complexes **1**−**14** in $CDCl_3$). Either the aromatic H_4-H_7 protons or the methyl protons of the 2,9-disubstituted phenanthroline ligand were monitored and used for the line-shape analysis of the spectra. The exchange rates were calculated using the computer program gNMR 4.0.[56] The activation parameters $\Delta H^{\ddagger}$ and $\Delta S^{\ddagger}$, together with $\Delta G^{\ddagger}$ (calculated at 340 K), were derived from a linear regression analysis of Eyring plots.

Crystallography. Crystals of [Pt(Me)(Me$_2$-phen)(PMe$_2$(C$_6$H$_5$))](BArf), **8**, [Pt(Me)(Me$_2$-phen)(P(*i*-Pr)$_3$)](BArf), **11**, [Pt(Me)(Me$_2$-phen)(PCy$_3$)](BArf), **14**, and of [Pt(Me)(phen)(P(C$_6$H$_5$)$_3$)](PF$_6$), **15**, suitable for X-ray diffraction, were obtained by crystallization from dichloromethane-*n*-hexane solutions and are air stable. All crystals were mounted on a Bruker SMART diffractometer, equipped with a CCD detector, for the unit cell and space group determinations. Crystals **11** and **15** were cooled, using a cold nitrogen stream, to 153(2) and 183(2) K, respectively, for the data collection, while for **8** and **14** data were collected at room temperature.

Experimental parameters and selected crystallographic and other relevant data are listed in Table 5 and in the Supporting Information (as a CIF file). Data were corrected for Lorentz and polarization factors with the data reduction software SAINT[57] and empirically for absorption using the SADABS program.[58] The structures were solved by Patterson and Fourier methods and refined by full matrix least squares[59] (the function minimized being $\sum[w(F_o^2 - (1/k)F_c^2])^2]$). To improve convergence, the C−F distances in the BArf moiety at room temperature were constrained to be approximately equal. For all structures, no extinction correction was deemed necessary. The scattering factors used, corrected for the real and imaginary parts of the anomalous dispersion, were taken from the literature.[60] The standard deviations on intensities were calculated in terms of statistics alone. All calculations were carried out by using the PC version of the programs WINGX,[61] SHELX-97,[59] and ORTEP.[62]

Structural Study of [Pt(Me)(Me$_2$-phen)(PMe$_2$(C$_6$H$_5$))](BArf), 8. From the lattice symmetry, the space group was assumed to be $P\bar{1}$ and later confirmed by the successful refinement. The cell constants were refined by least squares at the end of the data collection using 965 reflections ($\theta_{max} \leq 25.2°$). The BArf anion shows, as expected, large amplitude vibrational displacements and disorder in four of the eight substituted phenyl rings that could be modeled satisfactorily assuming two different orientations for the CF_3 groups, as obtained from difference Fourier maps. The two orientations were refined using anisotropic displacement parameters for the F atoms; the occupancy factors for the two different orientations are approximately equal (in the range 0.47−0.65). All other atoms were refined using anisotropic displacement parameters, except for the hydrogens; their contribution (calculated positions, C−H = 0.95(Å), B(H) = 1.3/1.5 × B(C_{bonded})(Å^2), 1.5 was used for the CH_3 groups) was included in the refinement using a riding model. Upon convergence, no significant features were found in the Fourier difference map.

Structural Study of [Pt(Me)(Me$_2$-phen)(P(*i*-Pr)$_3$)](BArf), 11. The space group was assumed to be $P\bar{1}$ and confirmed by the

(56) *gNMR*, version 4.0; Cherwell Science: Oxford, 1997.
(57) *BrukerAXS*, *SAINT*, Integration Software; Bruker Analytical X-ray Systems: Madison, WI, 1995.
(58) Sheldrick, G. M. *SADABS*, Program for Absorption Correction; University of Göttingen: Göttingen, Germany, 1996.
(59) Sheldrick, G. M. *SHELX-97*, Structure Solution and Refinement Package; Universität Göttingen: Göttingen, Germany, 1997.
(60) *International Tables for X-ray Crystallography*; Wilson, A. J. C., Ed.; Kluwer Academic Publisher: Dordrecht, The Netherlands, 1992; Vol. C.
(61) Farrugia, L. J. *J. Appl. Crystallogr.* **1999**, *32*, 837−838.
(62) Farrugia, L. J. *J. Appl. Crystallogr.* **1997**, *30*, 565.

successful refinement. The cell constants (at 153K) were refined by least squares at the end of the data collection using 918 reflections ($\theta_{max} \leq 21.2°$). The apparent large values of the ADPs for the CF_3 groups and the C1L carbon atom show the presence of disorder. However, the presence of split positions was not shown in the difference Fourier maps. Therefore, the anisotropic model was retained. Anisotropic displacement parameters were used for all atoms except the hydrogens. The hydrogen atoms, in their calculated positions (C−H = 0.95(Å), B(H) = 1.3/1.5 × B(C_{bonded})-(Å^2), 1.5 was used for the CH_3 groups), were included in the refinement using a riding model. Upon convergence, the final difference Fourier map showed no significant peaks.

Structural Study of [Pt(Me)(Me_2-phen)(PCy_3)](BArf) 14. The *Aba*2 space group was assumed, being consistent with the systematic absences; the choice was confirmed by the successful refinement. The cell constants were refined by least squares at the end of the data collection using 979 reflections ($\theta_{max} \leq 19.9°$). The BArf anion shows disorder in two of the eight substituted phenyl rings that could be modeled satisfactorily assuming, for the CF_3 groups, two different orientations (obtained from difference Fourier maps). The two orientations were refined using anisotropic displacement parameters for the disordered C atoms; with occupancy factors for the two carbons of 0.64 and 0.60, respectively. All other atoms were refined using anisotropic displacement parameters. The contribution of the hydrogen atoms, in their calculated positions (C−H = 0.95(Å), B(H) = 1.3/1.5 × B(C_{bonded})(Å^2)), was included in the refinement using a riding model. Refining the Flack's parameter tested the handedness of structure (cf. Table 5).[63] Upon convergence, no significant features were found in the Fourier difference map.

Structural Study of [Pt(Me)(phen)($P(C_6H_5)_3$)](PF_6), 15. The space group was unambiguously determined from the systematic absences, while the cell constants (at 183 K) were refined by least squares at the end of the data collection using 1012 reflections ($\theta_{max} \leq 25.3°$). For the refinement, anisotropic displacement parameters were used for all "heavy" atoms, while the hydrogen atoms, in their calculated positions (C−H = 0.95(Å), B(H) = 1.3/1.5 × B(C_{bonded})-(Å^2)), were included in the refinement using a riding model. Upon convergence, the final Fourier difference map showed no significant peaks.

Acknowledgment. We are grateful to a reviewer for suggestions and to the Ministero dell' Università e della Ricerca Scientifica e Tecnologica (MURST), PRIN 2002 and PRA 2003, for funding this work.

Supporting Information Available: ORTEP figures of compounds **8**, **11**, **14**, and **15** showing the full numbering schemes and a figure showing the dependence of the Pt−N2 separation from the symmetric deformation coordinate (*S4″*); tables giving the temperature dependence of the rate constants (k_f/s^{-1}) and the associated activation parameters ($\Delta H^{\ddagger}$, $\Delta S^{\ddagger}$, and $\Delta G^{\ddagger}$) (PDFs); full crystallographic data are available as CIF file (CCDC nos. 255085−255088). This material is available free of charge via the Internet at http://pubs.acs.org.

IC0485920

(63) Flack, H. D. *Acta Crystallogr.* **1983**, *A 39*, 876−881.